

NASA TECHNICAL
MEMORANDUM



NASA TM X-1199

NASA TM X-1199

FACILITY FORM 602	N66-17889	
	(ACCESSION NUMBER)	(THRU)
	47	1
	(PAGES)	(CODE)
	TMX-1199	01
	(NASA CR OR TMX GR AD NUMBER)	(CATEGORY)

HIGH-LIFT CHARACTERISTICS OF
A VARIABLE-SWEEP SUPERSONIC
TRANSPORT MODEL WITH A
BLENDED ENGINE-FUSELAGE AND
ENGINE-MOUNTED HORIZONTAL TAILS

by Vernard E. Lockwood
Langley Research Center
Langley Station, Hampton, Va.

GPO PRICE \$ _____

CFSTI PRICE(S) \$ 2.00

Hard copy (HC) _____

Microfiche (MF) 50

ff 653 July 65

HIGH-LIFT CHARACTERISTICS OF A VARIABLE-SWEEP SUPERSONIC
TRANSPORT MODEL WITH A BLENDED ENGINE-FUSELAGE
AND ENGINE-MOUNTED HORIZONTAL TAILS

By Vernard E. Lockwood

Langley Research Center
Langley Station, Hampton, Va.

NATIONAL AERONAUTICS AND SPACE ADMINISTRATION

For sale by the Clearinghouse for Federal Scientific and Technical Information
Springfield, Virginia 22151 - Price \$2.00

HIGH-LIFT CHARACTERISTICS OF A VARIABLE-SWEEP SUPERSONIC

TRANSPORT MODEL WITH A BLENDED ENGINE-FUSELAGE

AND ENGINE-MOUNTED HORIZONTAL TAILS

By Vernard E. Lockwood
Langley Research Center

SUMMARY

11881

An investigation has been made at low speed to determine the high-lift longitudinal and lateral stability and pitch control characteristics of a model of a proposed supersonic transport airplane configuration designated SCAT 14. Single- and double-slotted flaps in combination with a leading-edge slat were studied as a means of producing high lift. Other geometric variables studied were wing sweep and deflection of the fixed area of the model between the fuselage and the movable wing. Lateral stability data are included for one configuration. The investigation was made in the Langley 300-MPH 7- by 10-foot tunnel at a Mach number of 0.125 which corresponds to a Reynolds number based on the fuselage length of 6.52×10^6 .

The results showed that the model with the wing-fuselage flap at 70° sweep was longitudinally stable to near maximum lift coefficient; above this lift coefficient, however, pitch-up tendencies appeared depending on trailing-edge flap geometry and wing-fuselage flap geometry. Increasing the loading on the wing either by changing from single-slotted flaps to double-slotted flaps or by increasing the flap deflection beyond 30° resulted in greater pitch-up tendencies. Changing the wing-fuselage flap sweep from 70° to 75° resulted in instability near maximum lift.

Although downward deflection of the wing-fuselage flap did not eliminate the pitch-up tendency, it increased the range of lift coefficients over which stability existed. The maximum trimmed lift coefficient obtained with the wing at 13.5° sweep was approximately equal to $21 C_{L\alpha}$, where $C_{L\alpha}$ is the slope of the lift curve at zero lift coefficient for the wing without flaps. Several trailing-edge flap configurations gave about the same drag-due-to-lift factor as the wing without flaps for part of the lift range. With the double-slotted flap deflected 50° and the wing-fuselage flap deflected 45° , the model had directional stability beyond the angle of attack for maximum lift.

2011

INTRODUCTION

This paper presents the results of a low-speed investigation to determine the high-lift characteristics of a proposed variable-sweep supersonic transport configuration designated SCAT 14. A previous investigation (ref. 1) showed that the model with trailing-edge flaps undeflected had longitudinal stability about the wing pivot location for all wing sweep angles. A reduction in stability occurred, however, at angles of attack greater than 8° . Experience has indicated that further reductions in stability could be expected from the configuration with deflected trailing-edge flaps.

The combination of trailing-edge flaps and highly swept inboard fairing incorporated in the supersonic transport configuration tends to increase flow separation over the wings and reduce the horizontal-tail contribution to stability at high angles of attack. As a means of controlling separation, a slat was used along the full span of the movable wing and a deflected leading-edge flap was used on the fairing between the movable wing and the fuselage. The deflected flap not only should reduce the separation problem but also should increase the horizontal-tail contribution to stability, as indicated in reference 1. Single- and double-slotted flap configurations were investigated.

Longitudinal stability and control data were obtained for several configurations through an angle-of-attack range from about 0° to about 20° . Lateral-stability data were obtained for one model configuration through a range of sideslip angles from -5° to 15° . The investigation was made in the Langley 300-MPH 7- by 10-foot tunnel at a Mach number of 0.125 which corresponds to a Reynolds number based on fuselage length of 6.52×10^6 . The results of the investigation are presented without discussion.

SYMBOLS

Measurements for this investigation were taken in the U.S. Customary System of Units. Equivalent values are indicated herein parenthetically in the International System (SI) in the interest of promoting use of this system in future NASA reports. Details concerning the use of SI, together with physical constants and conversion factors, are given in reference 2.

The force and moment data contained herein are referred to the axis system shown in figure 1. The reference dimensions used in reducing the data based on the 75° swept wing are area, 7.00 square feet (0.6503 square meter); chord, 31.36 inches (0.7965 meter); and span, 38.25 inches (0.9716 meter). The moment reference point is located at the wing pivot station (fuselage station 50.00 inches (1.2700 meters)).

- b wing span
- c local airfoil chord

C_D drag coefficient, $\frac{\text{Drag}}{qS}$

C_L lift coefficient, $\frac{\text{Lift}}{qS}$

$C_{L\alpha}$ lift-curve slope at $\alpha = 0^\circ$, per deg

C_l rolling-moment coefficient, $\frac{\text{Rolling moment}}{qSb}$

$$C_{l\beta} = \frac{(C_{l,\beta=5^\circ} - C_{l,\beta=-5^\circ})}{\Delta\beta}$$

C_m pitching-moment coefficient, $\frac{\text{Pitching moment}}{qS c_{\text{ref}}}$

C_n yawing-moment coefficient, $\frac{\text{Yawing moment}}{qSb}$

$$C_{n\beta} = \frac{(C_{n,\beta=5^\circ} - C_{n,\beta=-5^\circ})}{\Delta\beta}$$

c_{ref} reference chord

C_Y side-force coefficient, $\frac{\text{Side force}}{qS}$

$$C_{Y\beta} = \frac{(C_{Y,\beta=5^\circ} - C_{Y,\beta=-5^\circ})}{\Delta\beta}$$

q dynamic pressure

S reference wing area

α angle of attack of fuselage reference line, deg

β angle of sideslip, deg

$\Delta\beta$ increment in sideslip angle between $\beta = \pm 5^\circ$, corrected for balance and strut deflection, deg

δ_h horizontal-tail deflection (positive when trailing edge is down), deg

δ_{WF}	wing-fuselage flap deflection (positive when leading edge is down), deg
δ_{dsf}	double-slotted flap deflection, deg
δ_{ssf}	single-slotted flap deflection, deg
Λ	wing leading-edge sweep angle, deg
Configuration designations:	
r	round leading edge for wing-fuselage flap
s	sharp leading edge for wing-fuselage flap
WF	wing-fuselage flap (see fig. 5)

MODEL

The model configuration features a variable-sweep wing with an outboard pivot location, a four-engine side-by-side arrangement which blends into the fuselage at the rear of the model from a dummy inlet located beneath the fuselage, and horizontal surfaces mounted from the sides of the engine ducts. A three-view drawing of the wing is presented in figure 2 and photographs of the model mounted in the Langley 300-MPH 7- by 10-foot tunnel are shown in figure 3. Various model dimensions are given in tables I and II.

Fuselage cross sections drawn to model scale are presented in figure 4. It should be noted that the sections in the vicinity of the intake duct are solid, no provisions being made for internal flow.

The wing used in the present investigation had a planar lower surface and, with the exception of the flaps, is identical to wing 1 of reference 1. The airfoil sections of the wing were developed from an NACA 65A006 section by shearing the ordinates upward to provide a flat bottom except in the immediate vicinity of the leading edge. In this region the nose sections were rounded to provide a radius equal to 0.007 chord. (See table I for ordinates.)

The model was provided with replaceable fillets between the fuselage and the movable wing which served to provide changes in sweep, leading-edge contour, and deflection. Two of the fillets or wing-fuselage flaps are shown in figures 2 and 5 and figure 2 of reference 1. Each is described by the leading-edge sweep, the leading-edge contour (r = round; s = sharp), and the deflection of flap in a plane perpendicular to the hinge line (for example, $WF = 70^{\circ}s0^{\circ}$). Wing-fuselage flap $WF = 60.4^{\circ}r0^{\circ}$ was faired with a radius equal to one-half the thickness of the wing at the flap hinge line. (See fig. 5(b).) Other dimensions relating to the model, including dimensions of the horizontal and vertical tail, are given in table II and in figure 2.

Two high-lift systems were used in the investigation; typical sections for each are shown in figure 5. The single-slotted flap had a chord of 25 percent

of the airfoil chord and covered nearly the entire span of the movable wing. The double-slotted flap was a combination of the single-slotted flap and a 12.5-percent-airfoil-chord vane ahead of the flap. A 15-percent-chord slat was attached to the leading edge of the wing to aid in controlling separation. Ordinates for the flap and vane are given in tables III and IV, respectively. For a few tests with the double-slotted flap deflected 50° , the main flap was extended to the sides of the engine nacelle, as shown in figure 5(b). The vane was not extended for this extended-flap arrangement because of space limitations. During the tests, the slat leading-edge position, the slat trailing-edge gap, and the single-slotted flap gap were varied; the gaps and positions of the slat are indicated in figure 5 and also in each data plot. The numbers in the figure legends give the slat leading-edge position below the lower surface of the wing and the gap between the slat trailing edge and the wing. (For example, slat: 0.050c; 0.018c.)

TEST AND CORRECTIONS

The investigation was made in the Langley 300-MPH 7- by 10-foot tunnel with the model strut supported from the floor of the tunnel as shown in figure 3. Forces and moments were measured by an internally mounted six-component strain-gage balance attached to the support strut. To insure a turbulent boundary-layer transition, strips approximately $1/8$ inch wide (0.003 meter) of No. 100 carborundum grains were attached to the model surfaces at the 7-percent-chord station.

The investigation was made at a dynamic pressure of 22.9 pounds per square foot (1096 Newtons per square meter) which corresponds to a Mach number of 0.125 and a Reynolds number based on fuselage length of 6.52×10^6 . All configurations were investigated through a range of angle of attack to about 20° , and selected configurations were also investigated at sideslip angles of -5° , 5° , 10° , and 15° .

The drag data were corrected to correspond to a pressure at the base of the engine nacelles equal to free-stream static pressure. The jet-boundary corrections calculated for the drag and angle of attack by the method of reference 3 are as follows:

$$C_D = C_{D,\text{measured}} + (0.114C_L^2)$$

$$\alpha = \alpha_{\text{measured}} + (0.652C_L)$$

The jet-boundary corrections to the pitching-moment data were found to be negligible. The data were also corrected for wind-tunnel blockage by the method presented in reference 4. The angles of attack and sideslip were corrected for deflection of the balance and sting under load. The effect of the support strut on the model characteristics is unknown but because of the thinness of the strut it is thought that the corrections to the data would be small.

PRESENTATION OF DATA

The data obtained in the investigation are presented in the following figures:

	Figure
Longitudinal characteristics:	
Double-slotted flaps -	
Effect of flap extension and horizontal tail	6 to 7
Effect of flap deflection and horizontal tail	8 to 9
Effect of wing-fuselage flap deflection and geometry	10 to 12
Effect of wing sweep and horizontal tail	13 to 14
Effect of slat leading-edge position	15
Effect of slat trailing-edge gap	16
Single-slotted flaps -	
Effect of flap gap	17
Effect of leading-edge slats and single-slotted flap deflection	18
Summary of lift-drag characteristics	19
Lateral characteristics:	
Effect of vertical tail on stability derivatives	20
Effect of sideslip angle	21

SUMMARY OF RESULTS

An investigation of the high-lift characteristics of a variable-sweep supersonic transport model with a leading-edge slat and flaps on the leading and trailing edges of the movable wings has indicated the following results:

With the wing-fuselage flap at 70° sweep the model was longitudinally stable up to near maximum lift coefficient; above this lift coefficient, however, pitch-up tendencies appeared depending on trailing-edge flap geometry and the wing-fuselage flap geometry. Increasing the loading on the wing either by changing from single- to double-slotted flaps or by increasing the flap deflection beyond 30° resulted in greater pitch-up tendencies with little increase in maximum trimmed lift coefficient. An increase in the wing-fuselage flap sweep from 70° to 75° , which increased the wing area ahead of the moment reference (wing pivot station), also resulted in a pitch-up tendency, but at a much lower lift coefficient. Although downward deflection of the wing-fuselage flap did not eliminate the pitch-up tendency, it increased the range of lift coefficients over which stability existed.

The maximum trimmed lift coefficient obtained with the wing at 13.5° sweep was approximately equal to $21 C_{L\alpha}$, where $C_{L\alpha}$ is the slope of the lift curve (per degree) at a zero lift coefficient for the wing without flaps. A change in the wing leading-edge sweep from 13.5° to 25° resulted in a loss of about 9 percent in the maximum untrimmed lift coefficient. Several trailing-edge

flap configurations gave about the same drag-due-to-lift factor as the wing without flaps over a limited lift-coefficient range.

With the double-slotted flap deflected 50° and the 70° wing-fuselage flap deflected 45° , the model had directional stability beyond the angle of attack for maximum lift.

Langley Research Center,
National Aeronautics and Space Administration,
Langley Station, Hampton, Va., September 15, 1965.

REFERENCES

1. Lockwood, Vernard E.; and Thompson, Wilson E.: Low-Speed Characteristics of a Variable-Sweep Supersonic Transport Model With a Blended Engine Fuselage and Engine-Mounted Tails. NASA TM X-1038, 1964.
2. Mechtly, E. A.: The International System of Units - Physical Constants and Conversion Factors. NASA SP-7012, 1964.
3. Gillis, Clarence L.; Polhamus, Edward C.; and Gray, Joseph L., Jr.: Charts for Determining Jet-Boundary Corrections for Complete Models in 7- by 10-Foot Closed Rectangular Wind Tunnels. NACA WR L-123, 1945. (Formerly NACA ARR L5G31.)
4. Herriot, John G.: Blockage Corrections for Three-Dimensional-Flow Closed-Throat Wind Tunnels, With Consideration of the Effect of Compressibility. NACA Rept. 995, 1950. (Supersedes NACA RM A7B28.)

TABLE I.- WING ORDINATES

[Lower surface ordinates are all zero;
leading-edge radius = 0.700]

Percent chord	Upper surface ordinates, percent chord
0	0.700
.5	1.432
.75	1.525
1.25	1.615
2.5	1.990
5.0	2.620
7.5	3.182
10	3.648
15	4.388
20	4.948
25	5.374
30	5.648
35	5.890
40	5.992
45	5.984
50	5.850
55	5.586
60	5.204
65	4.728
70	4.174
75	3.550
80	2.874
85	2.166
90	1.454
95	.740
100	.026

TABLE II.- MODEL DIMENSIONS

Reference:

Area, sq ft (sq meter)	7.00	(0.6503)
Span, in. (meter)	38.25	(0.9716)
Chord, in. (meter)	31.36	(0.7965)

Fuselage:

Length, in. (meters)	89.00	(2.2606)
Base area of engine, sq ft (sq meter)	0.1365	(0.0127)

Horizontal tail:

Leading-edge sweep, deg	60.0	
Trailing-edge sweep, deg	28.6	
Root chord, in. (meter)	13.70	(0.3480)
Tip chord, in. (meter)	4.20	(0.1067)
Span (panel), in. (meter)	8.00	(0.2032)
Span (overall), in. (meter)	27.76	(0.7051)
Exposed area (total, sq ft) (sq meter)	0.970	(0.0901)

Vertical tail:

Leading-edge sweep, deg	70.0	
Trailing-edge sweep, deg	42.0	
Root chord, in. (meter)	22.52	(0.5720)
Tip chord, in. (meter)	4.60	(0.1168)
Span, in. (meter)	9.68	(0.2459)
Exposed area, sq ft (sq meter)	1.000	(0.0929)

WF = 70°s0°:

Area, sq ft (sq meter)	0.389	(0.0361)
----------------------------------	-------	----------

WF = 75°s0°:

Area, sq ft (sq meter)	0.714	(0.0663)
----------------------------------	-------	----------

WF = 60.4°r0°:

Area, sq ft (sq meter)	0.014	(0.0013)
----------------------------------	-------	----------

TABLE III.- FLAP ORDINATES

[Lower surface ordinates are all zero]

Percent chord	Upper surface ordinate, percent chord
0	0.55
0.50	1.21
1.00	1.48
2.00	1.87
3.00	2.15
4.00	2.36
5.00	2.48
6.00	2.56
7.00	2.55
8.00	2.44
9.00	2.30
10.00	2.17
25.00	.026

TABLE IV.- VANE ORDINATES

Percent chord	Upper surface ordinate, percent chord	Lower surface ordinate, percent chord
0	0	0
.156	.476	-.335
.313	.653	-.424
.625	.924	-.511
.938	1.131	-.557
1.250	1.300	-.560
1.875	1.586	-.511
2.500	1.800	-.375
3.750	2.038	-.175
5.000	2.075	.013
6.250	2.000	.225
7.500	1.800	.375
8.750	1.462	.400
10.000	1.038	.375
11.250	.563	.225
11.875	.325	.134
12.500	0	0

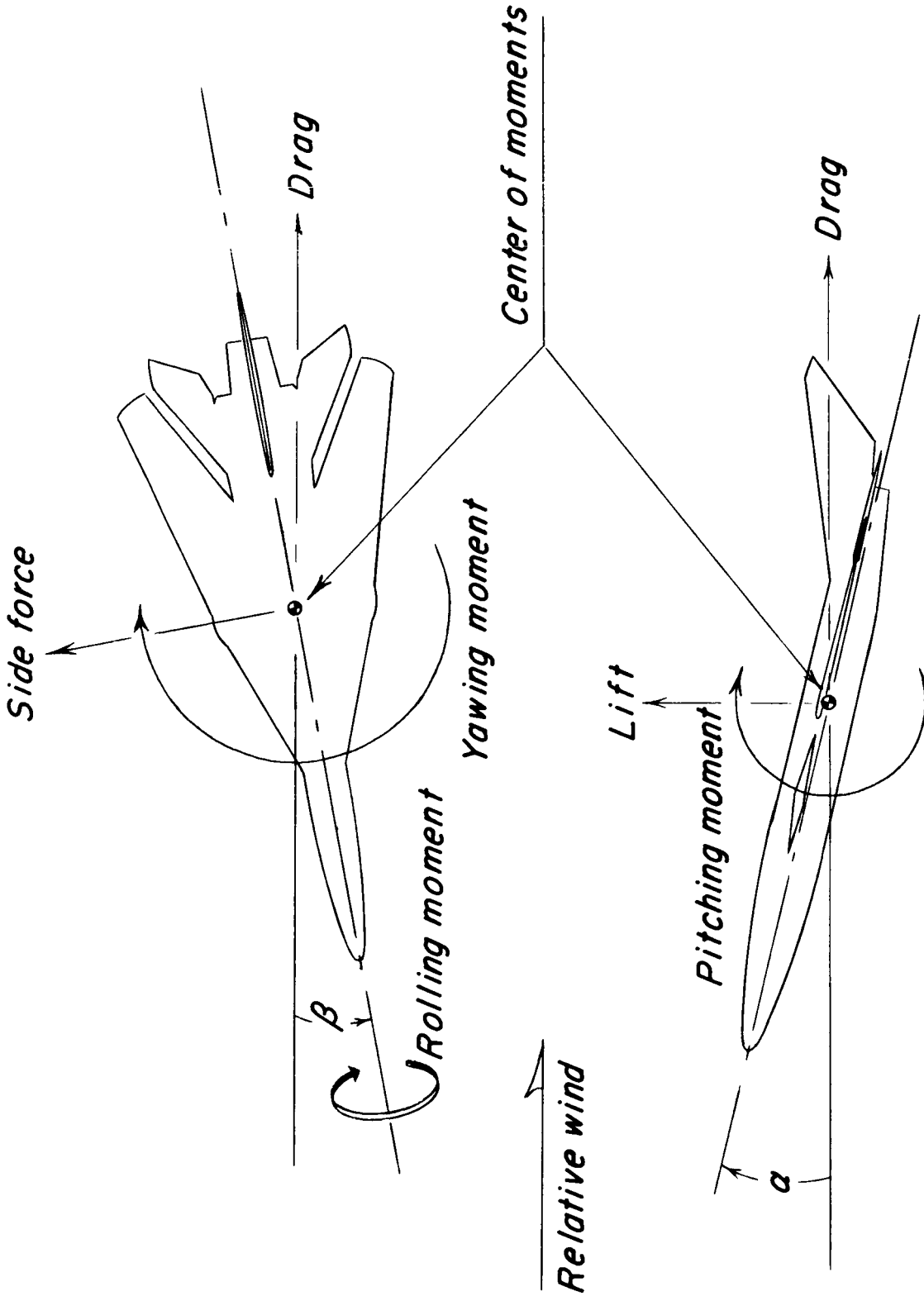


Figure 1.- Sketch of axis system used for presentation of data.

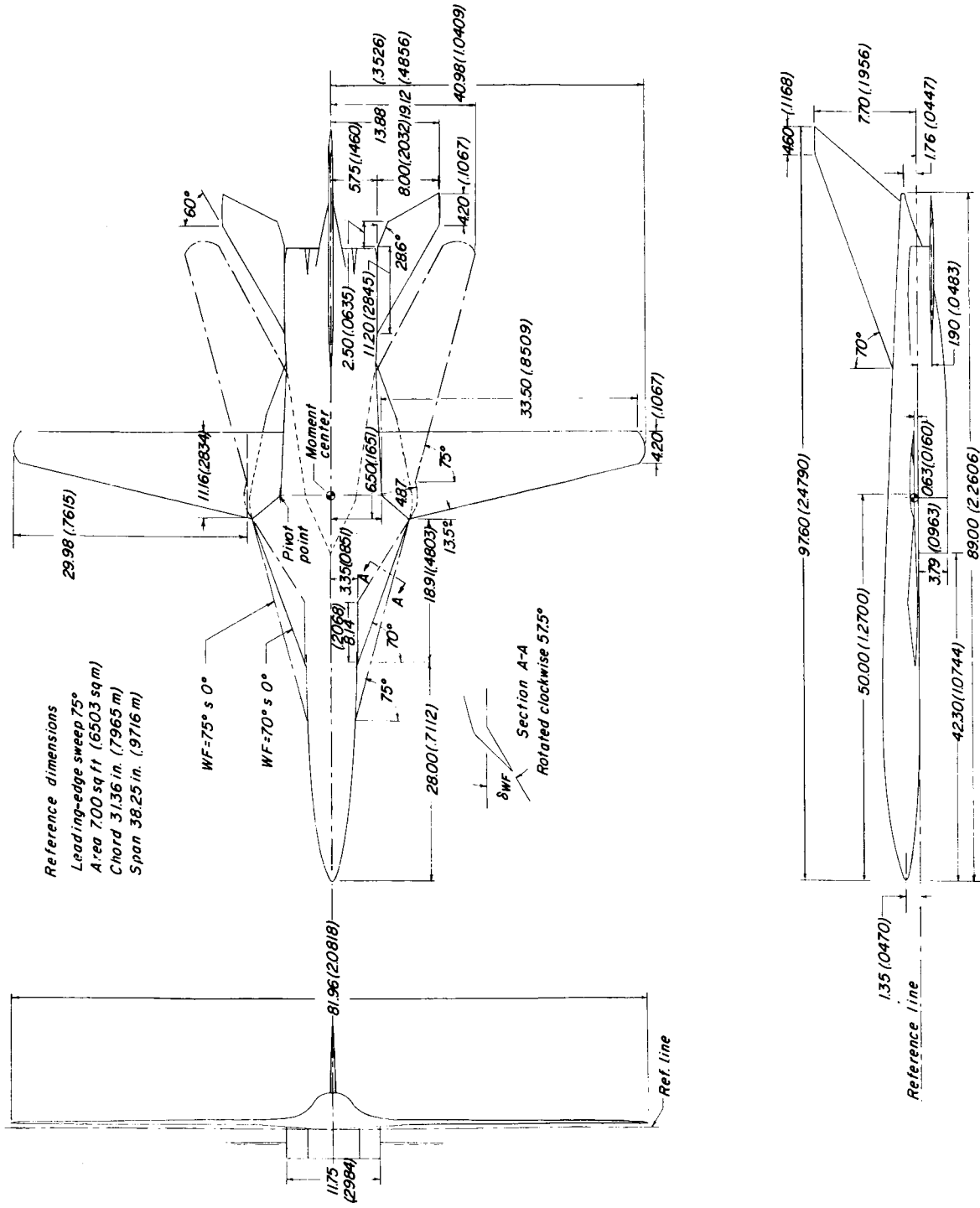
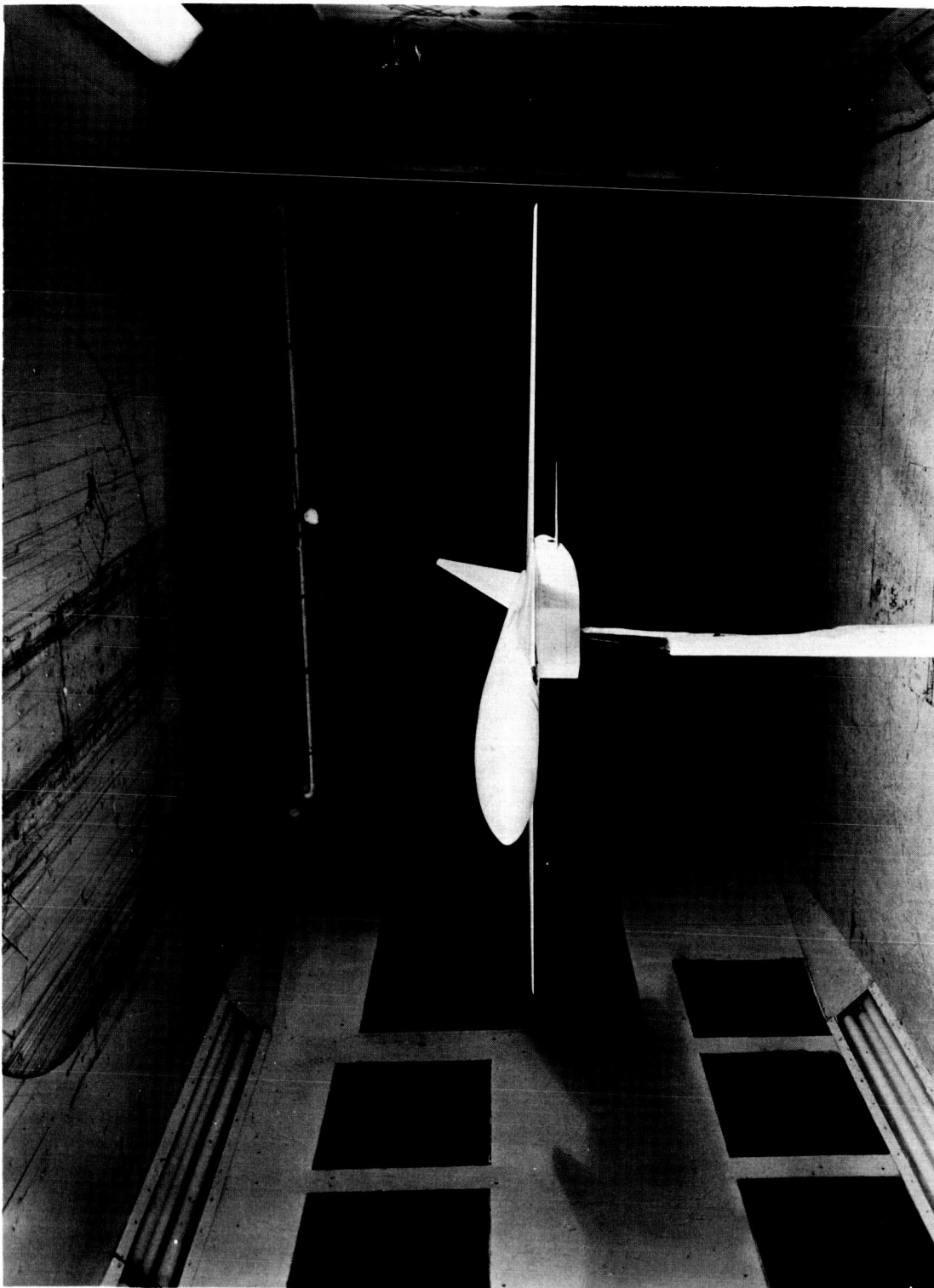


Figure 2.- Drawing of model tested. All linear dimensions are in inches and parenthetically in meters.



(a) Front view with wings fully extended (leading-edge sweep 13.5°).
Figure 3.- Model installed in Langley 300-MPH 7- by 10-foot tunnel.

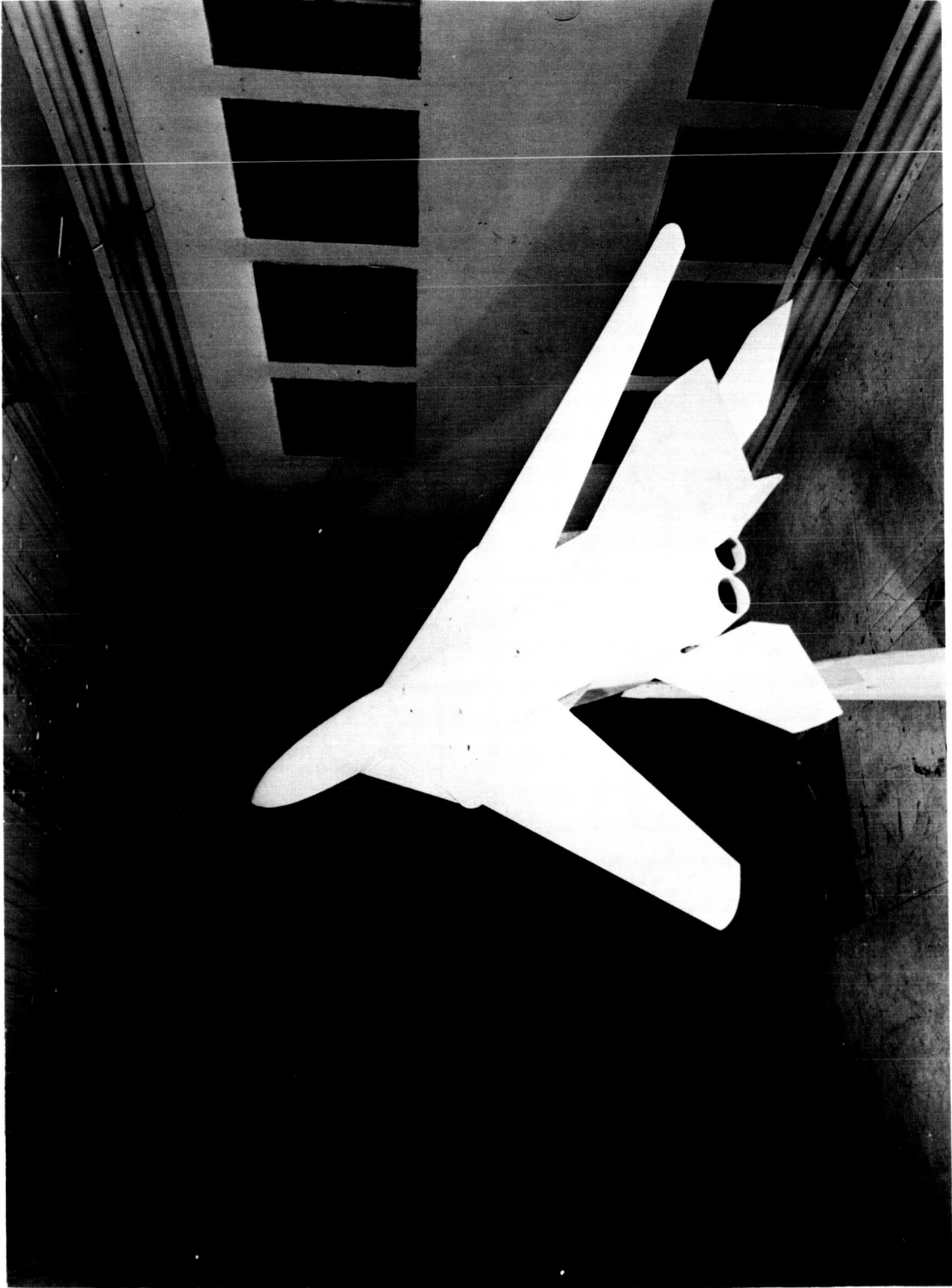
L-61-8078



L-61-8079

(b) Rear view with wings fully extended.

Figure 3.- Continued.



(c) Rear view with wing leading edges swept 65° .

Figure 3.- Concluded.

L-61-8080

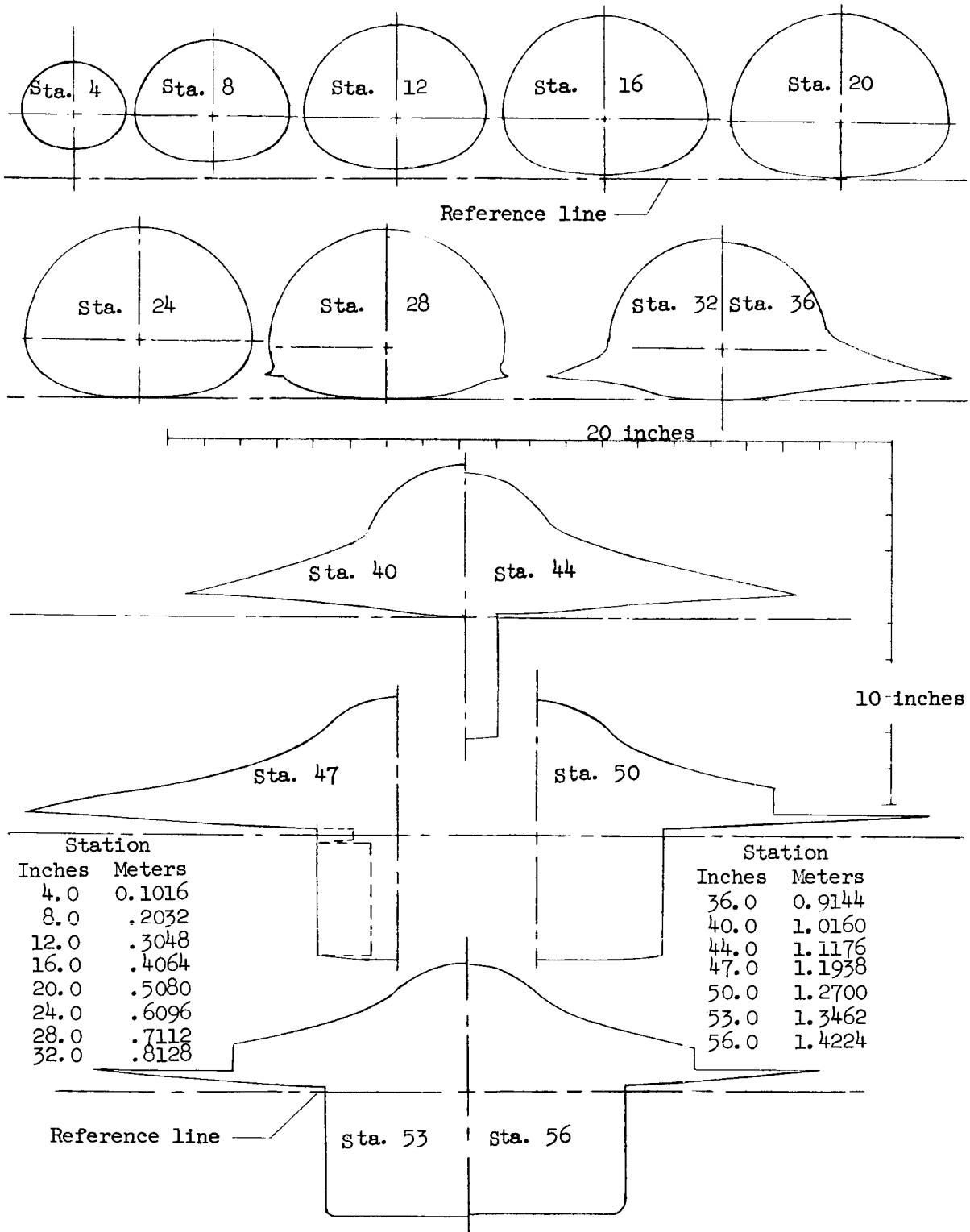


Figure 4.- Model fuselage cross sections.

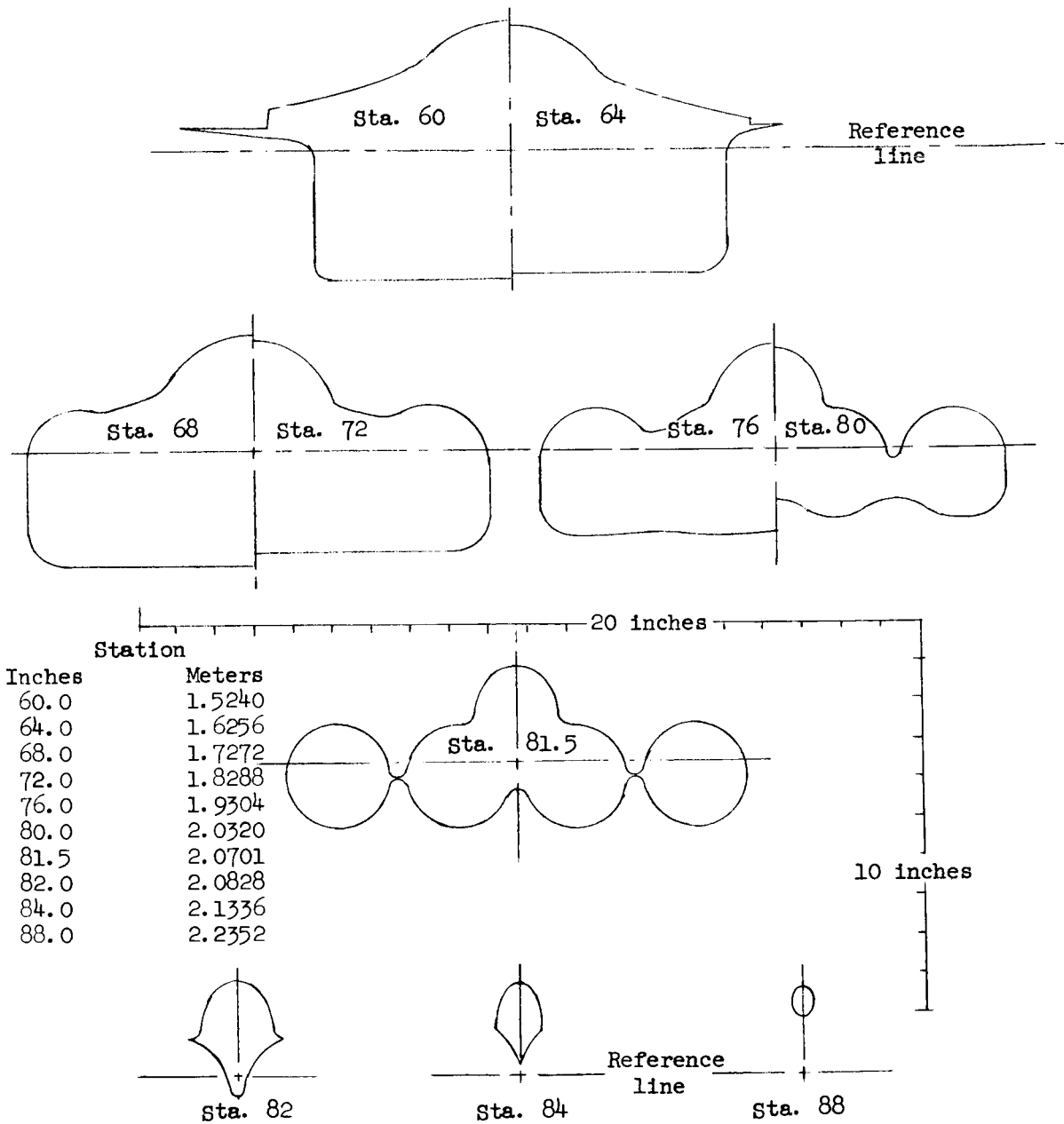
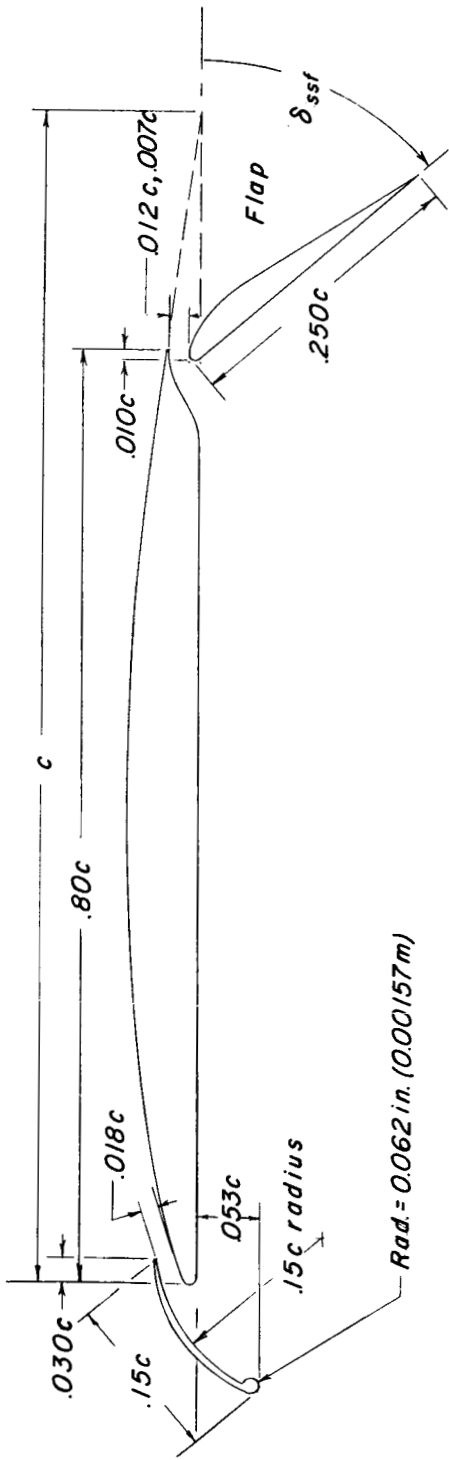
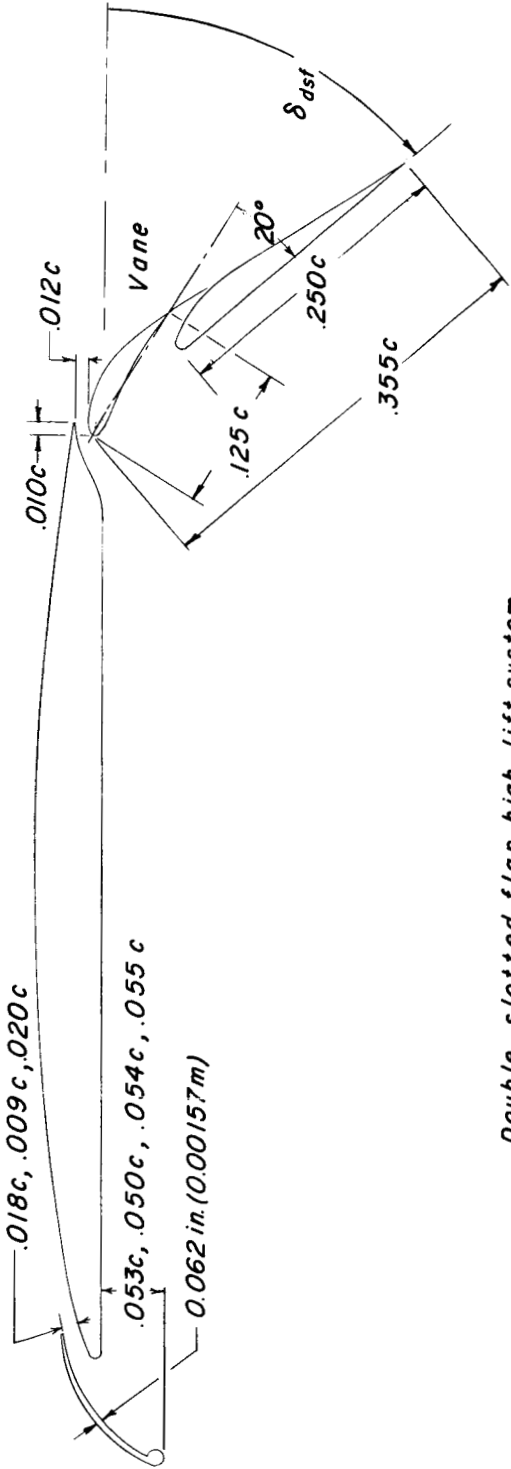


Figure 4.- Concluded.



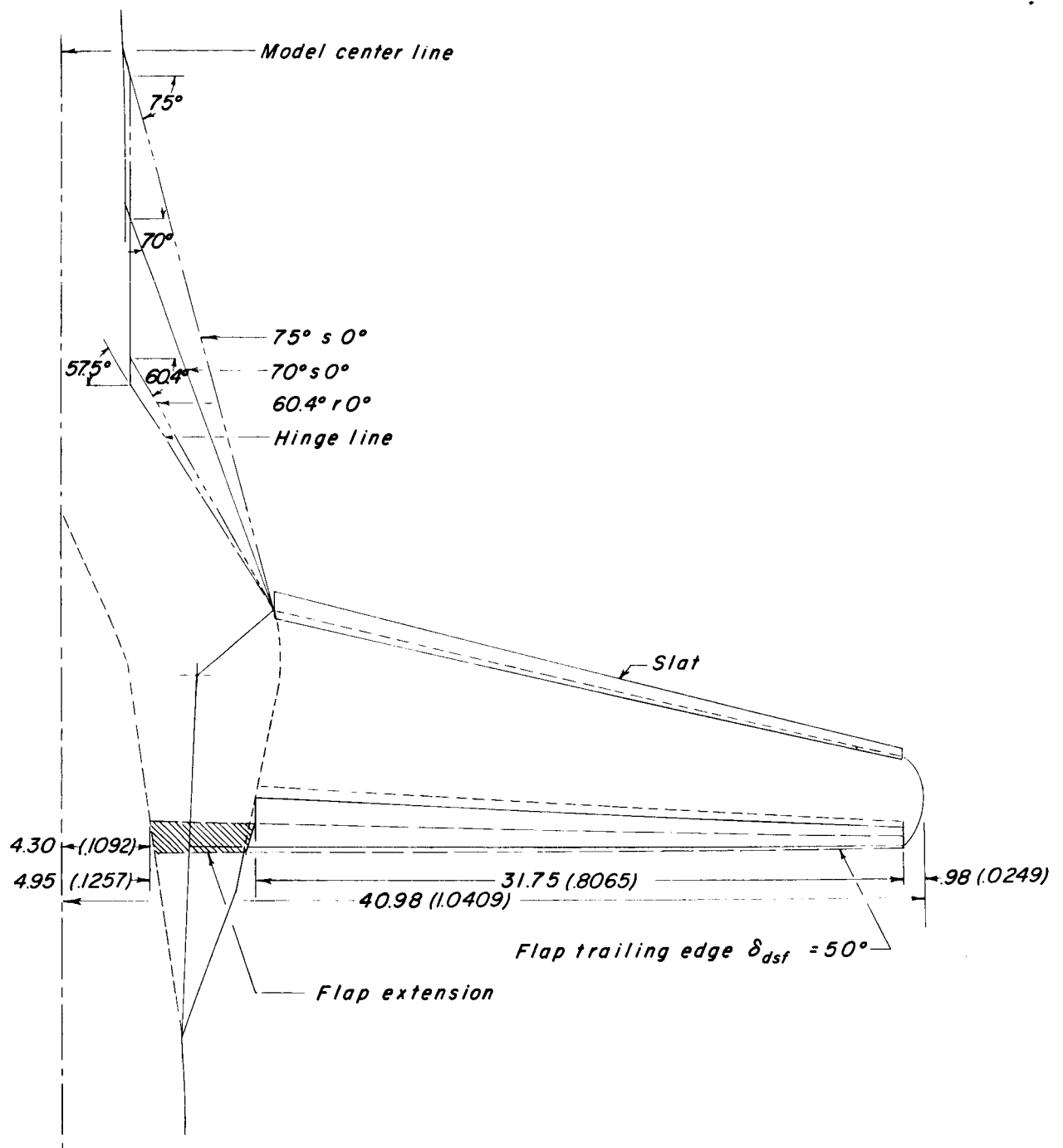
Single - slotted flap high - lift system



Double - slotted flap high - lift system

(a) Airfoil sections.

Figure 5.- Sketch of high-lift system. Dimensions are in inches and parenthetically in meters.



(b) Planform.

Figure 5.- Concluded.

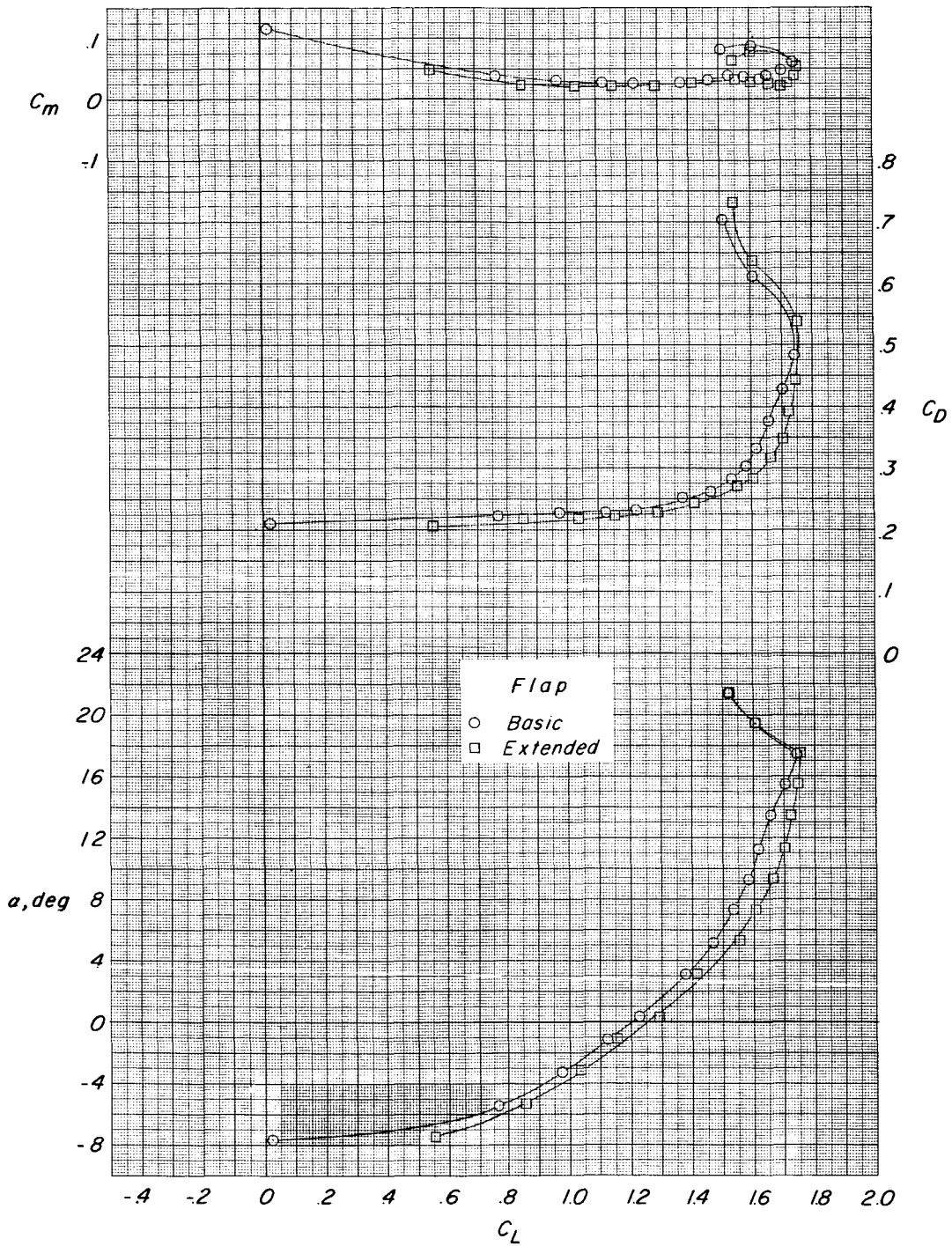
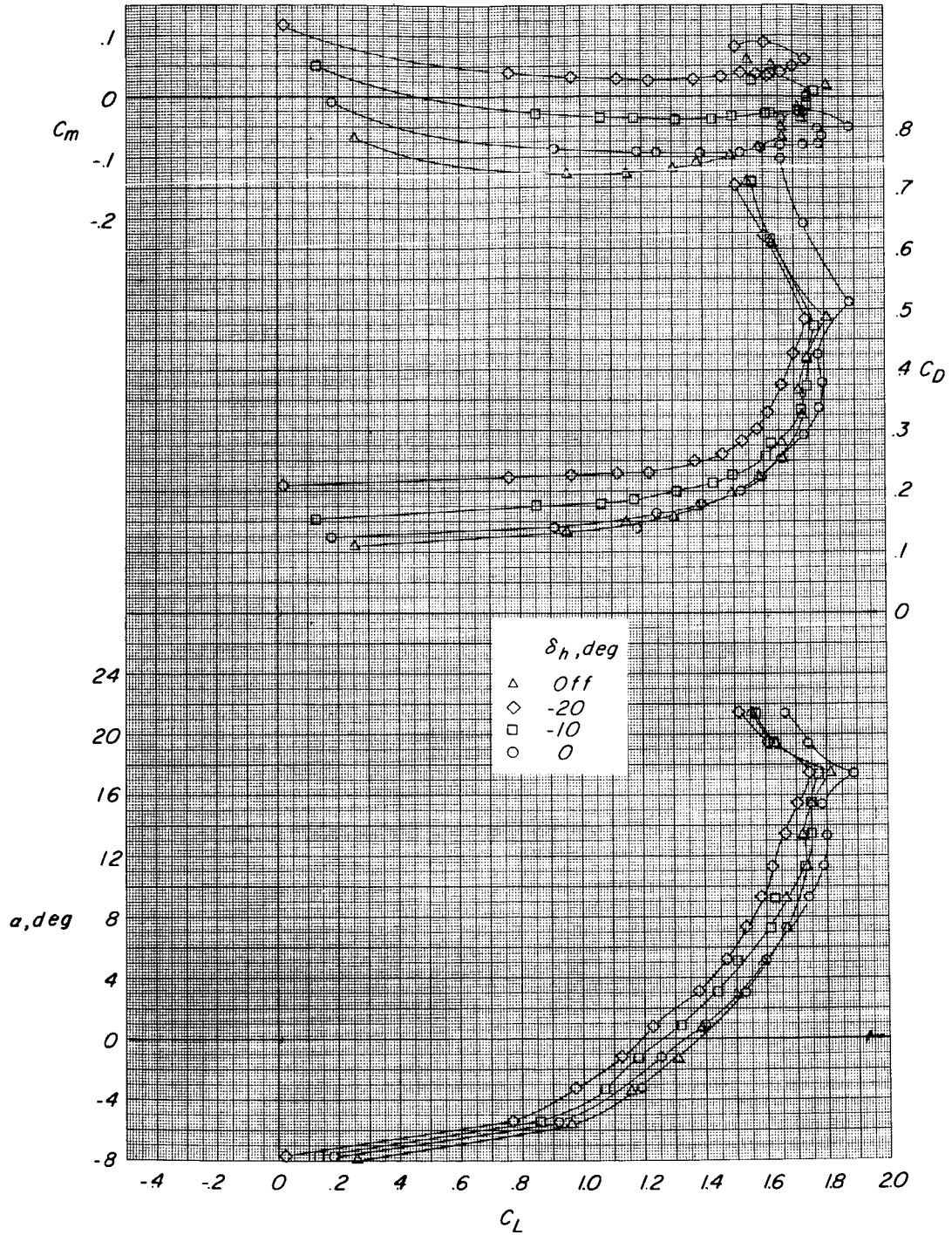
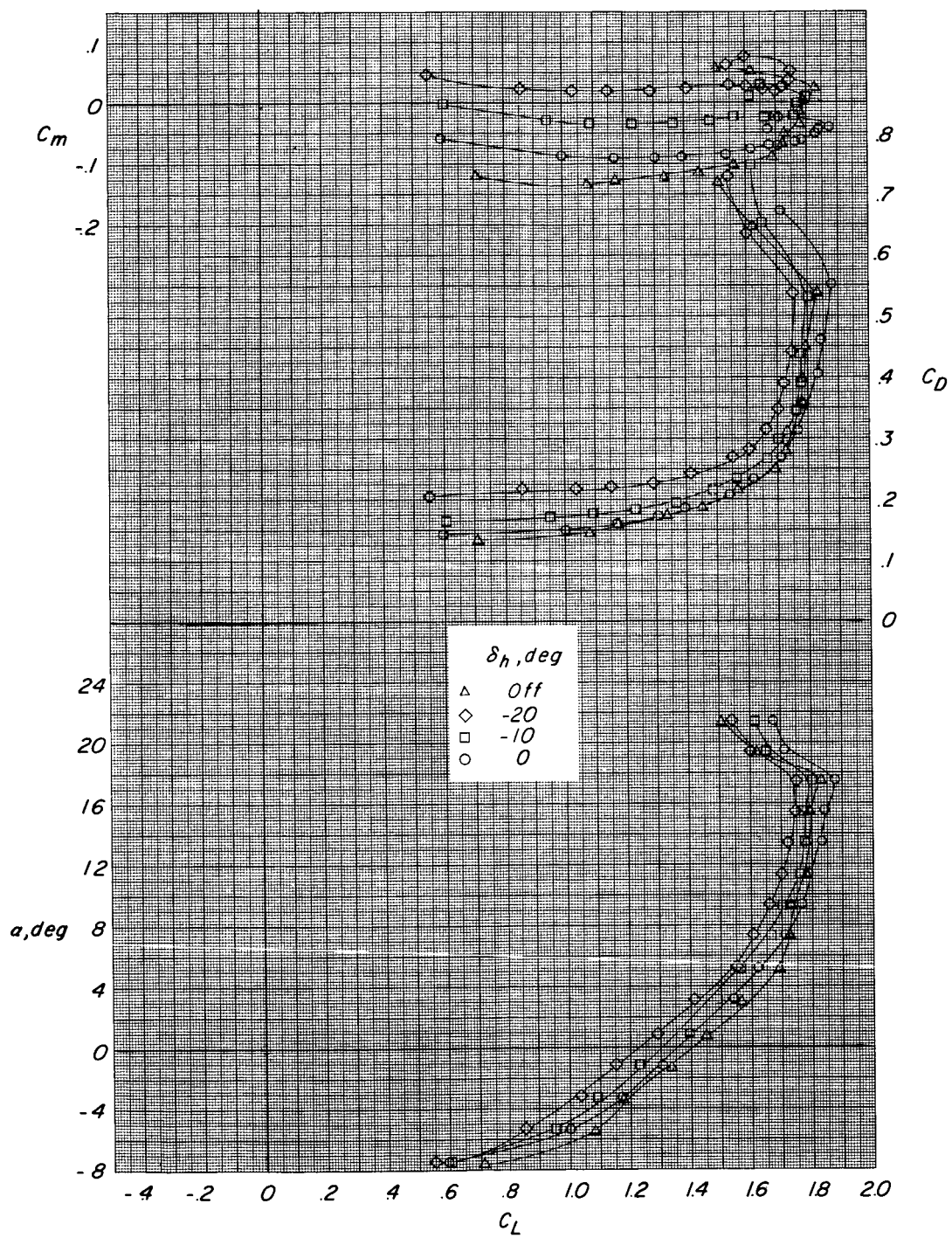


Figure 6.- Effect of flap extension. $\Lambda = 13.5^\circ$; $WF = 70^\circ s^\circ$;
 $\delta_h = -20^\circ$; slat: $0.053c$; $0.018c$; $\delta_{dsf} = 50^\circ$.



(a) Basic flaps.

Figure 7.- Effect of horizontal tail. $\Lambda = 13.5^\circ$; $WF = 70^\circ \text{so}^\circ$;
 slat: $0.053c$; $0.018c$; $\delta_{dsr} = 50^\circ$.



(b) Extended flaps.

Figure 7.- Concluded.

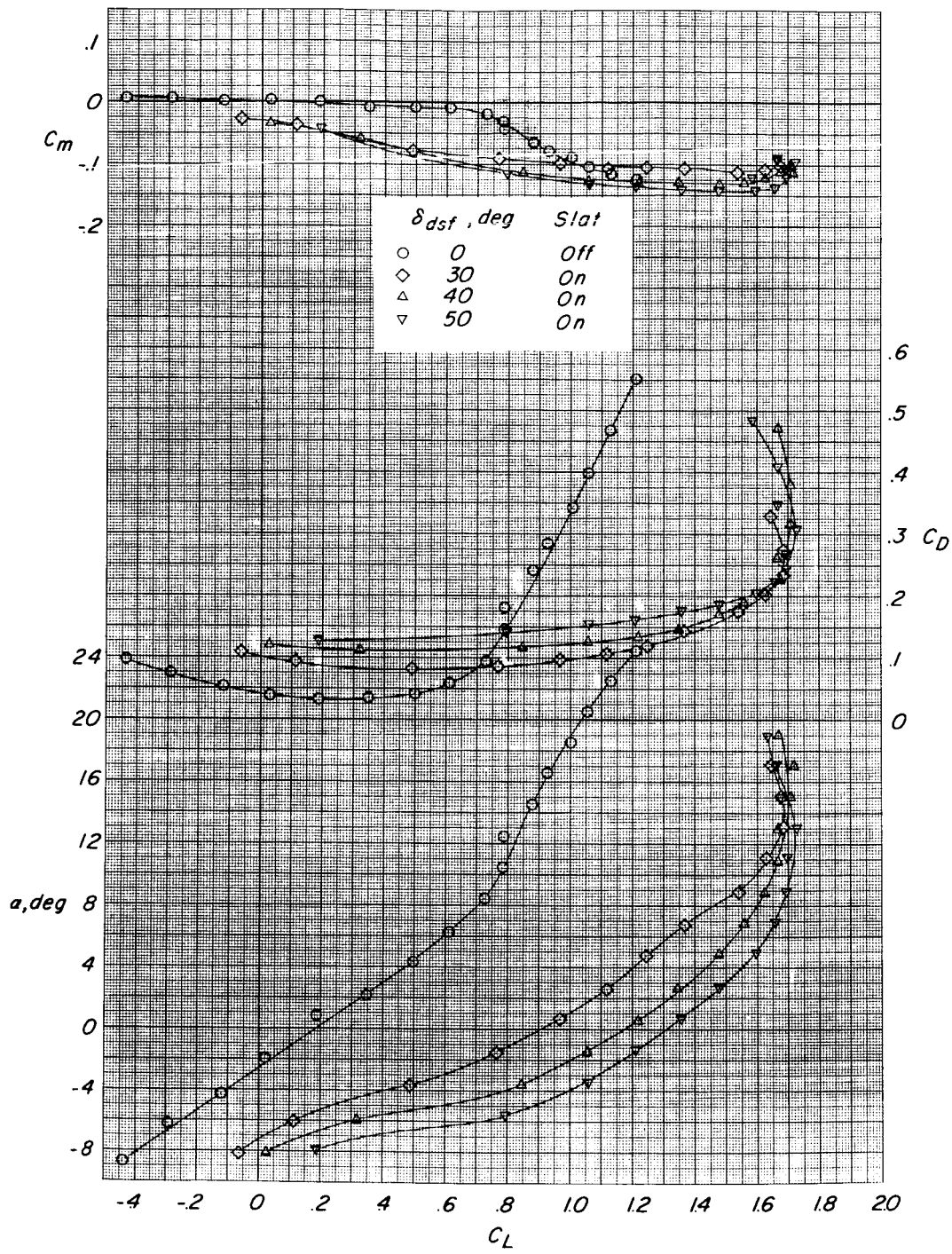
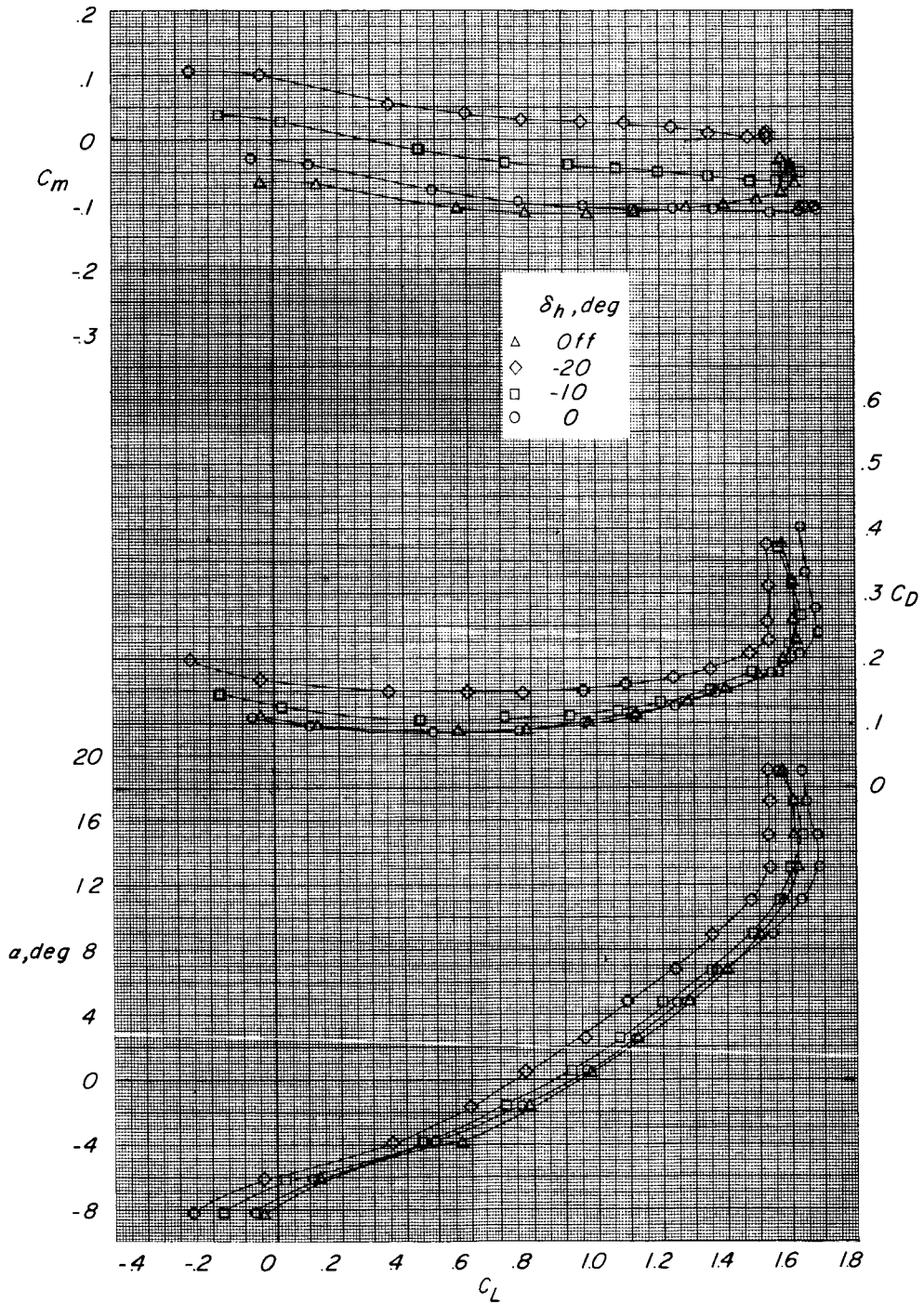
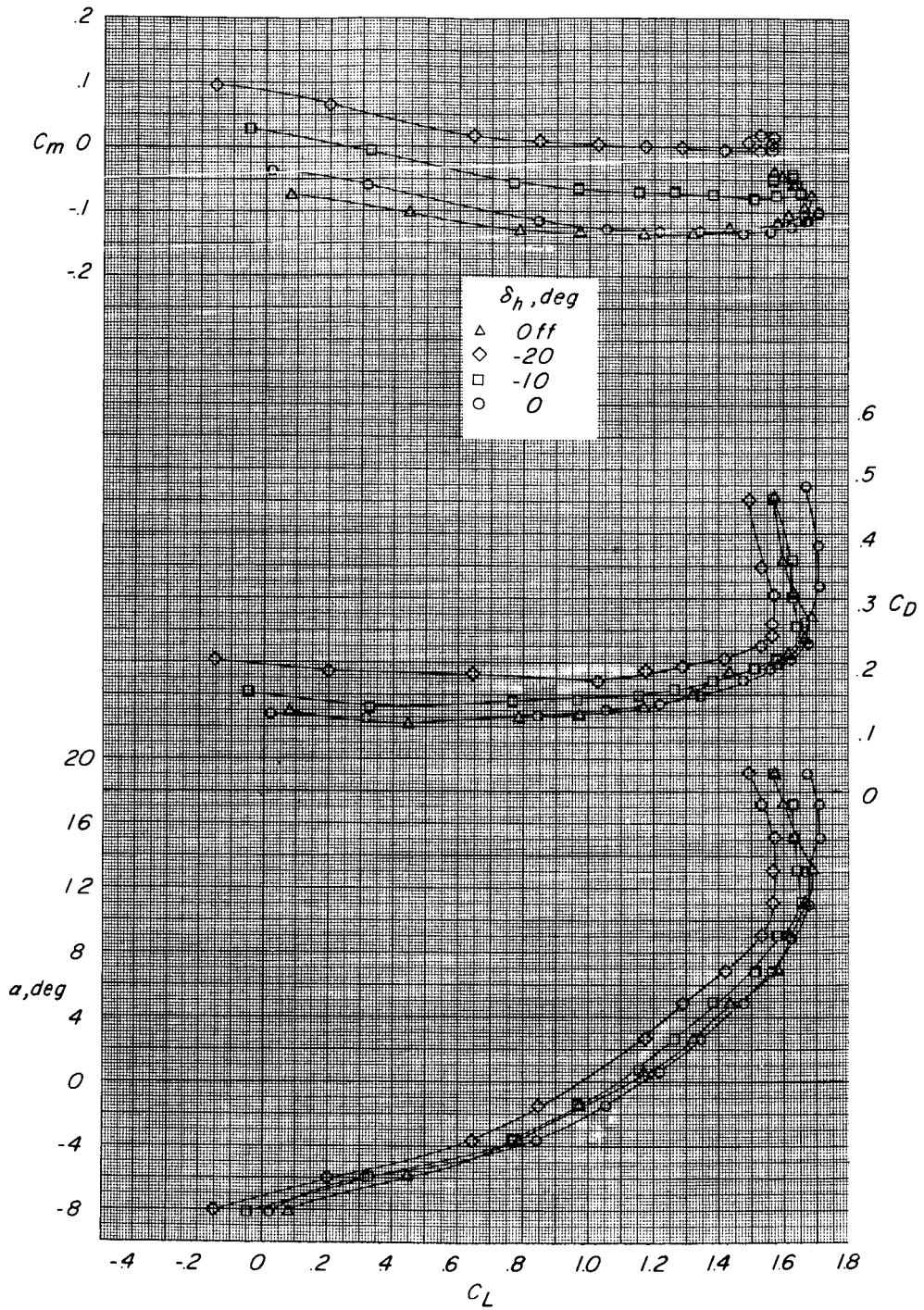


Figure 8.- Effect of double-slotted flap deflection. $\Lambda = 13.5^\circ$;
 $WF = 70^\circ s 45^\circ$; $\delta_h = 0^\circ$; slat: 0.050c; 0.020c.



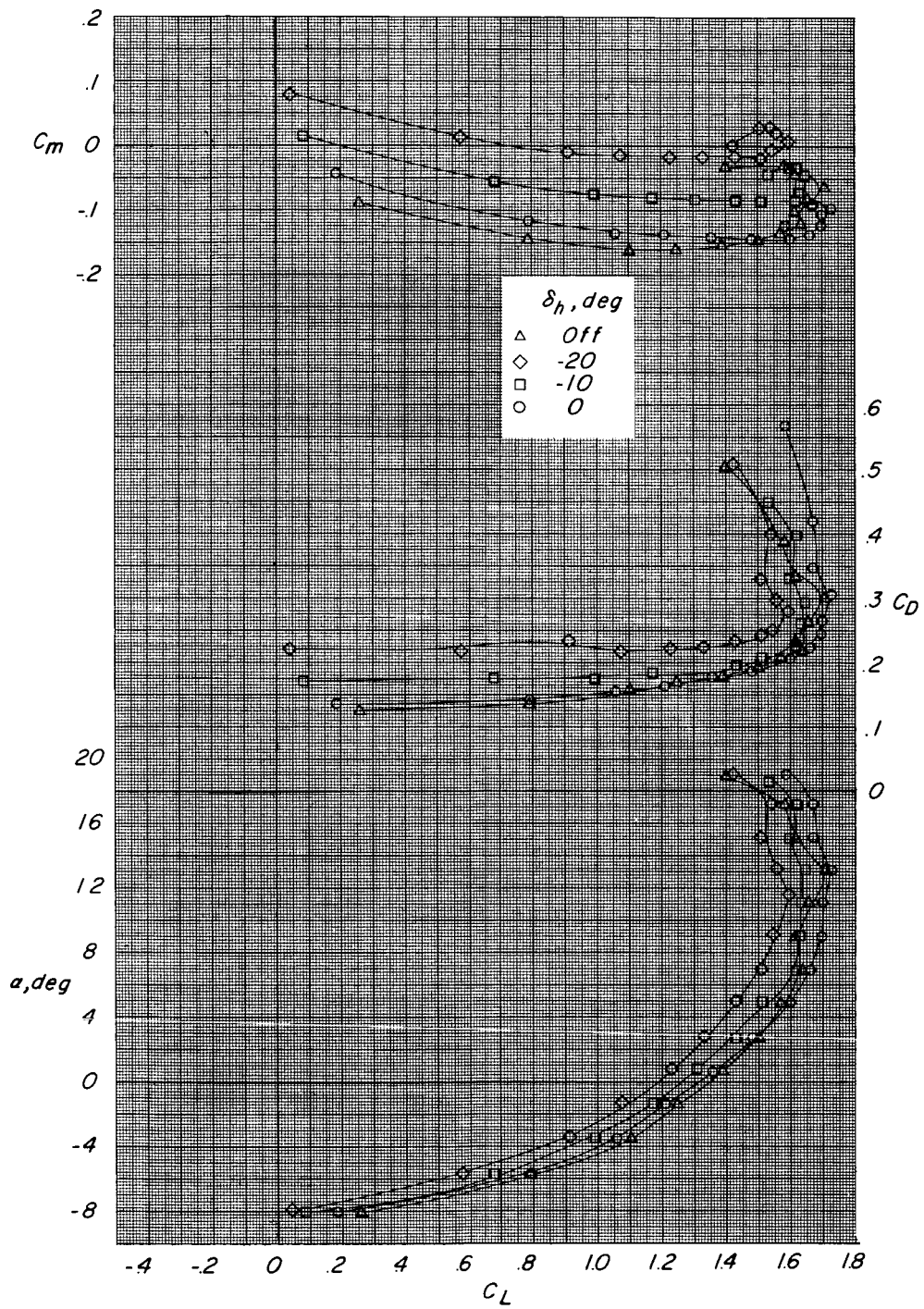
(a) $\delta_{dsf} = 30^\circ$.

Figure 9.- Effect of horizontal tail. $\Lambda = 13.5^\circ$;
 WF = $70^\circ s 45^\circ$; slat: 0.050c; 0.020c.



(b) $\delta_{dsr} = 40^\circ$.

Figure 9.- Continued.



(c) $\delta_{dsf} = 50^\circ$.

Figure 9.- Concluded.

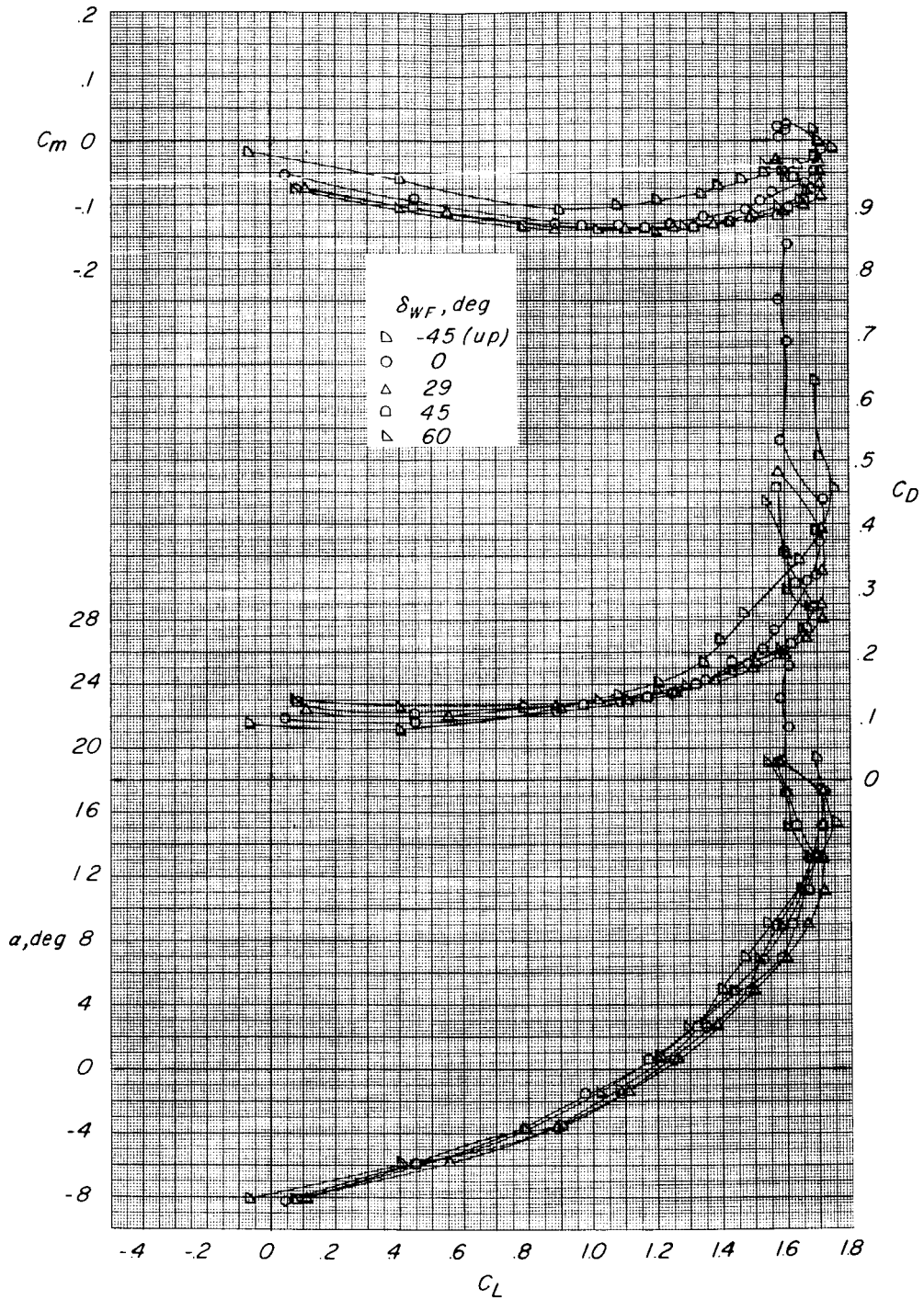
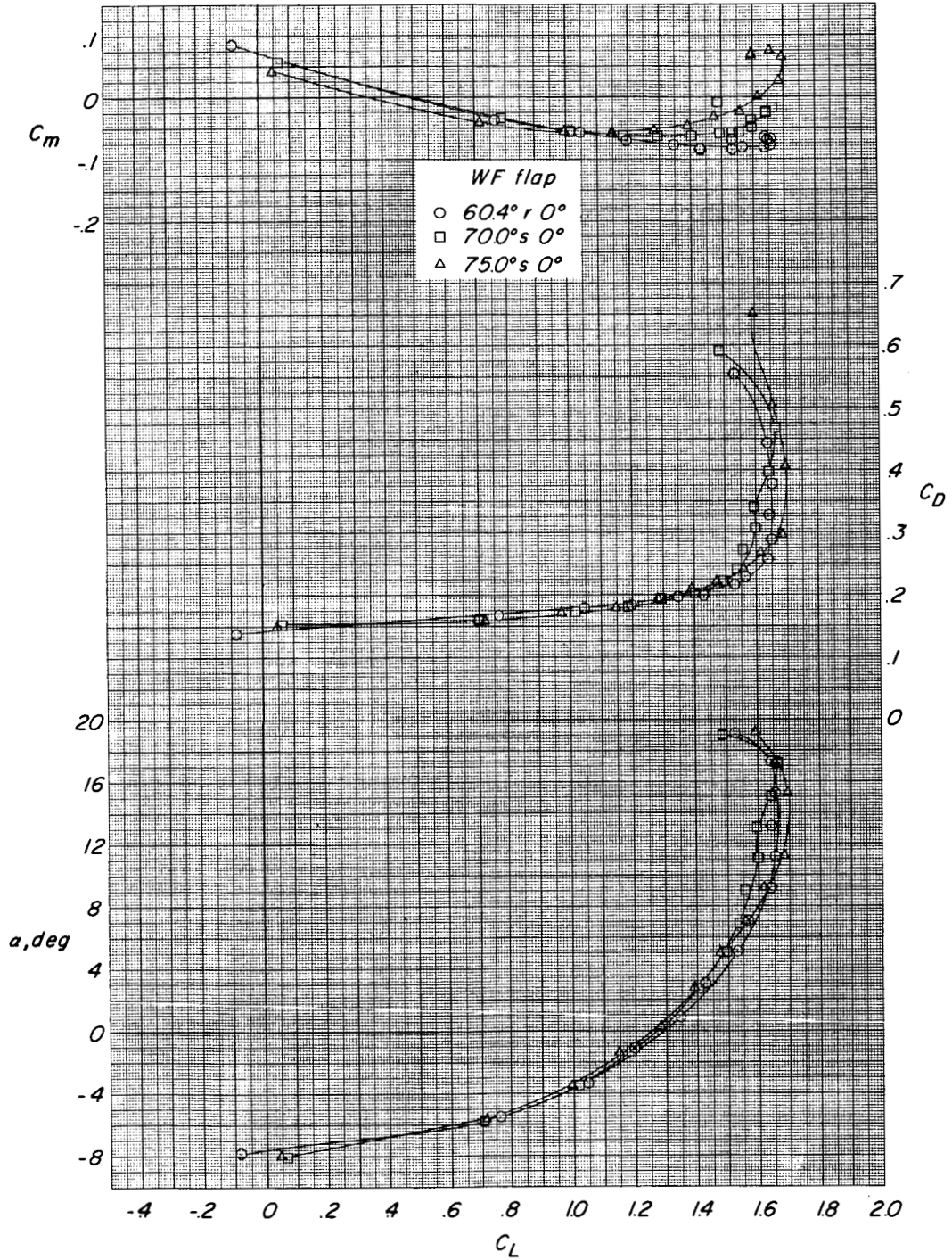
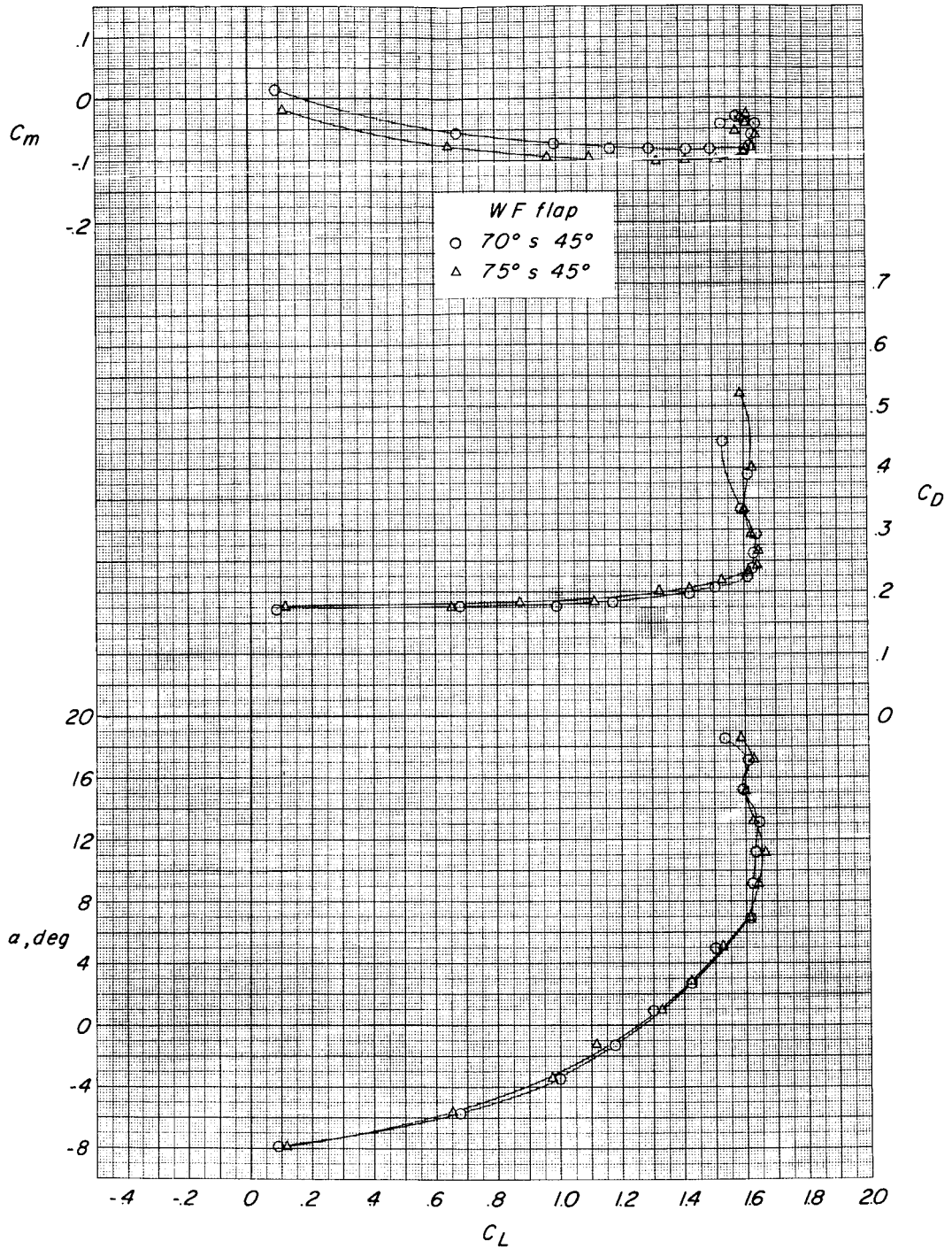


Figure 10.- Effect of wing-fuselage flap deflection. $\Lambda = 13.5^\circ$; horizontal tail off; slat: 0.050c; 0.020c; $\delta_{dsf} = 40^\circ$; WF = 70s.



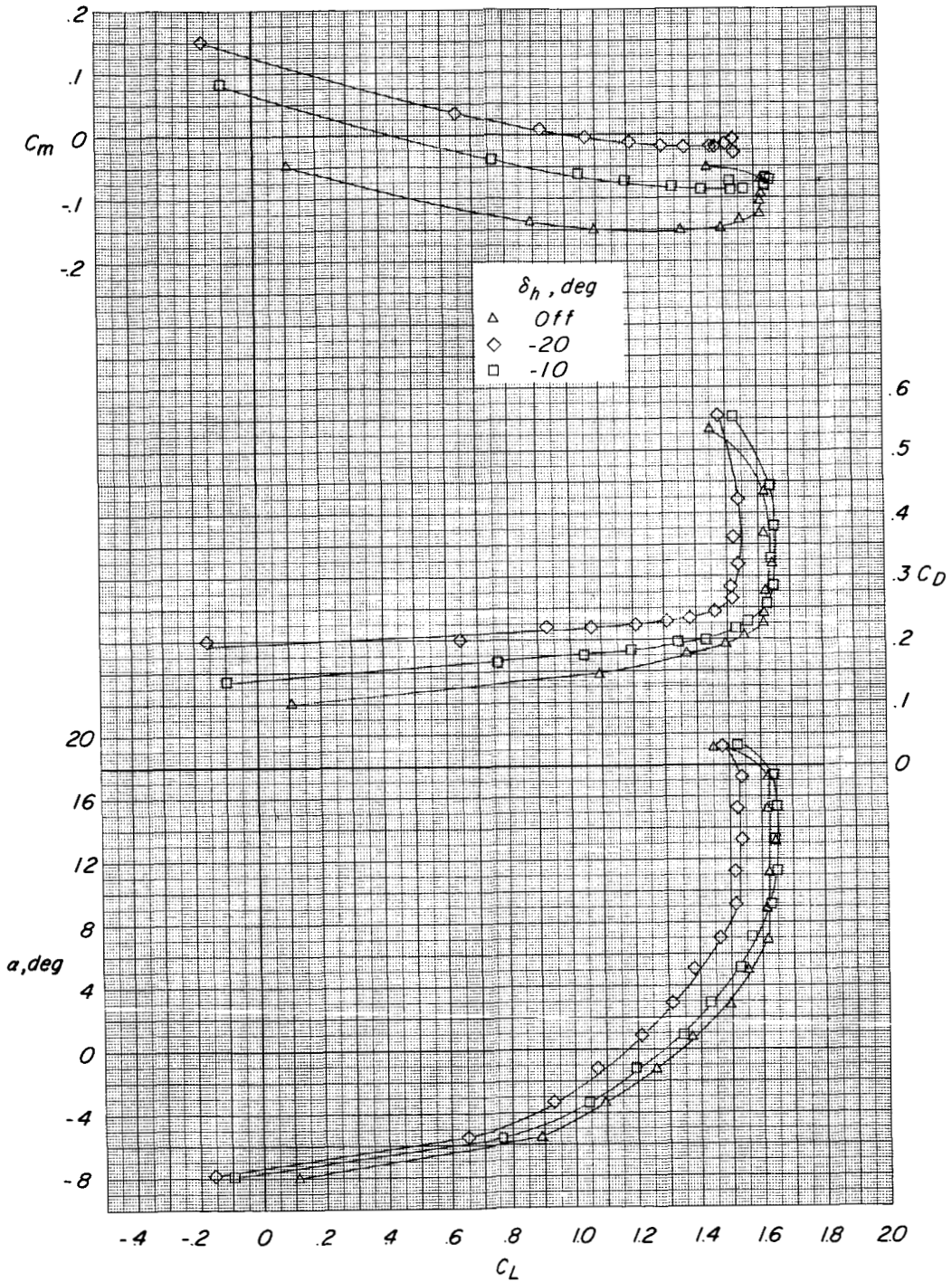
(a) $\delta_{WF} = 0^\circ$.

Figure 11.-Effect of wing-fuselage flap geometry. $\Lambda = 13.5^\circ$; $\delta_n = -10^\circ$; slat: $0.050c$; $0.020c$; $\delta_{dsf} = 50^\circ$.



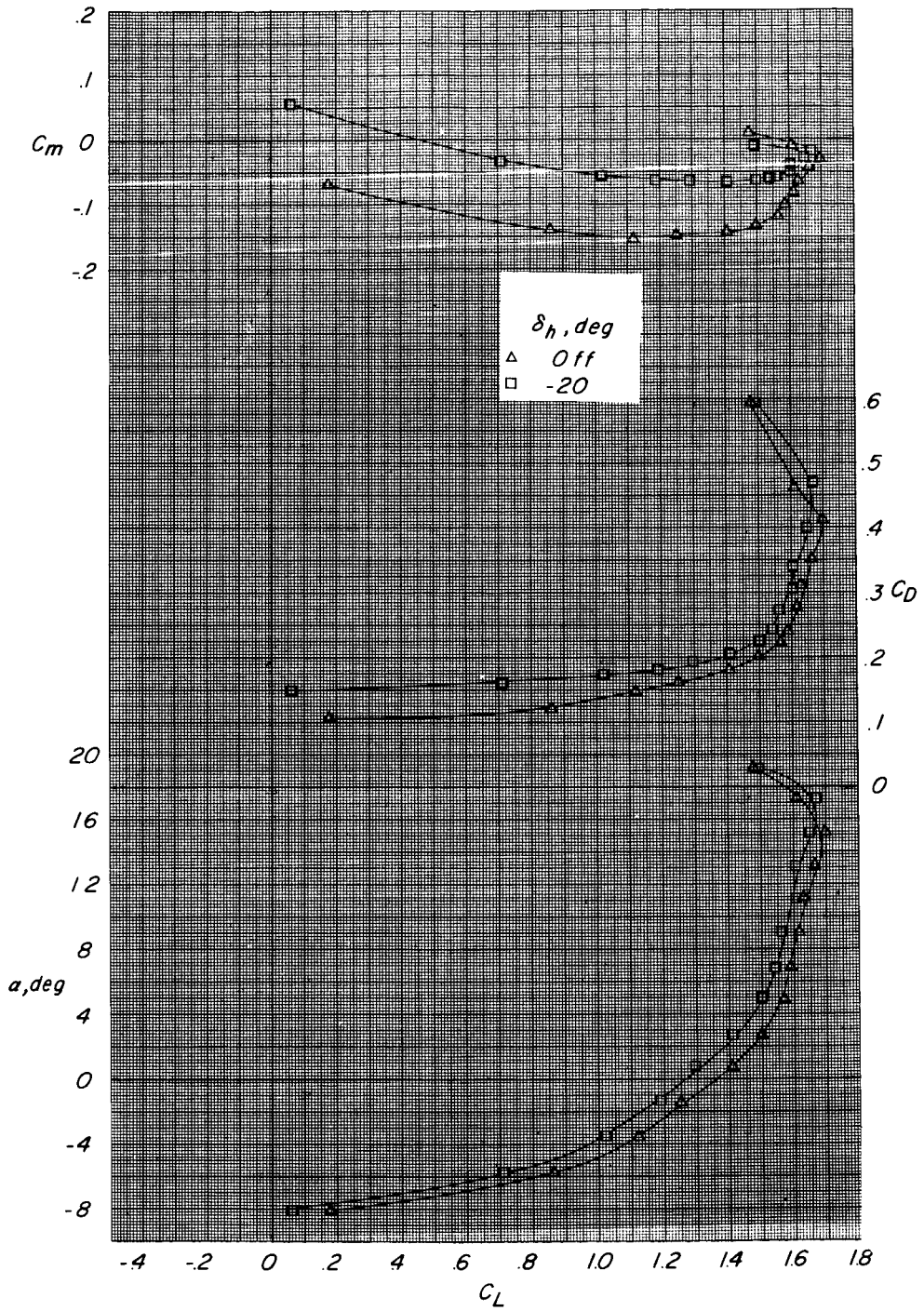
(b) $\delta_{WF} = 45^\circ$.

Figure 11.- Concluded.



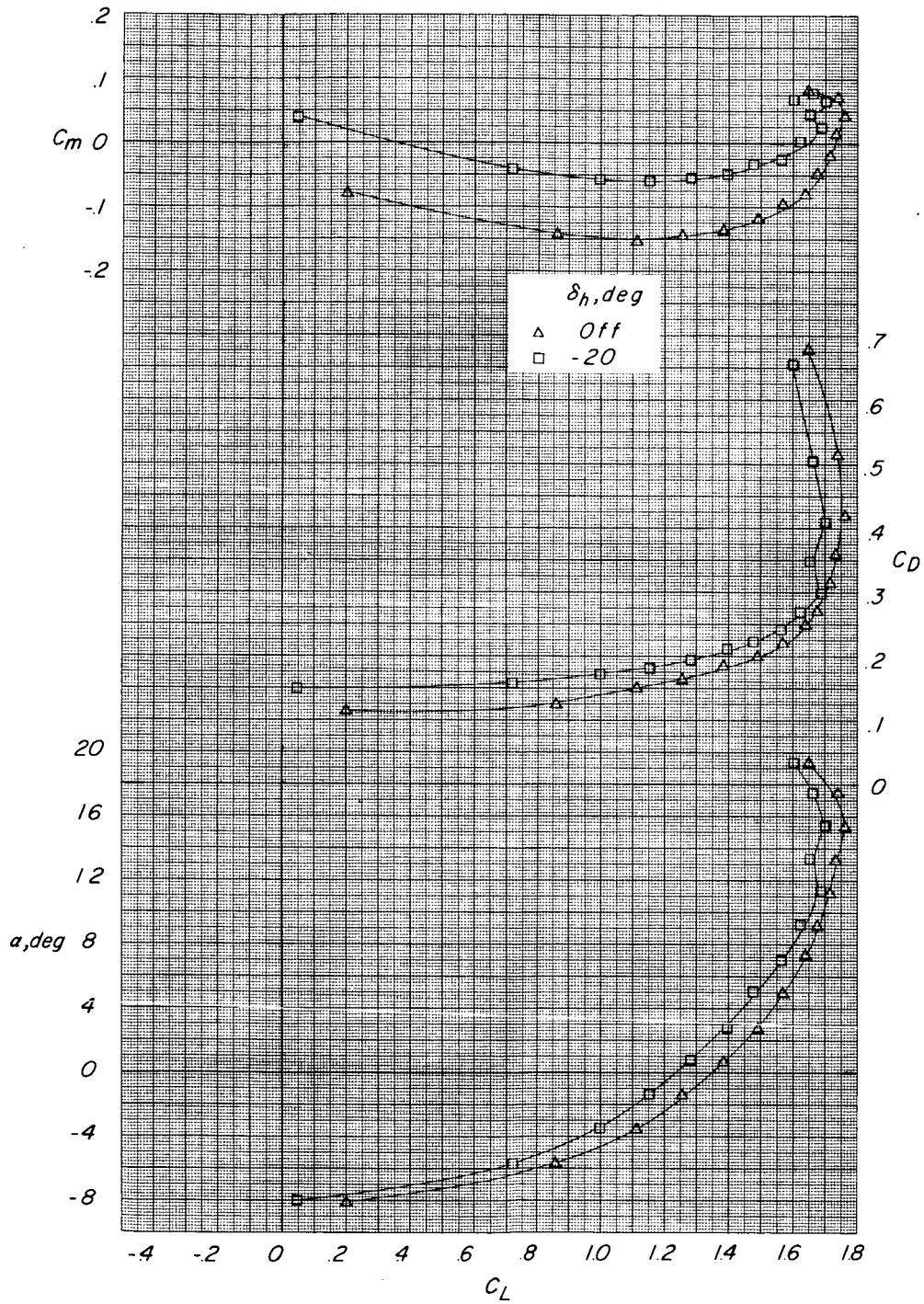
(a) $WF = 60.4r0^\circ$.

Figure 12.- Effect of horizontal tail. $\Lambda = 13.5^\circ$; slat: $0.050c$; $0.020c$; $\delta_{dsf} = 50^\circ$.



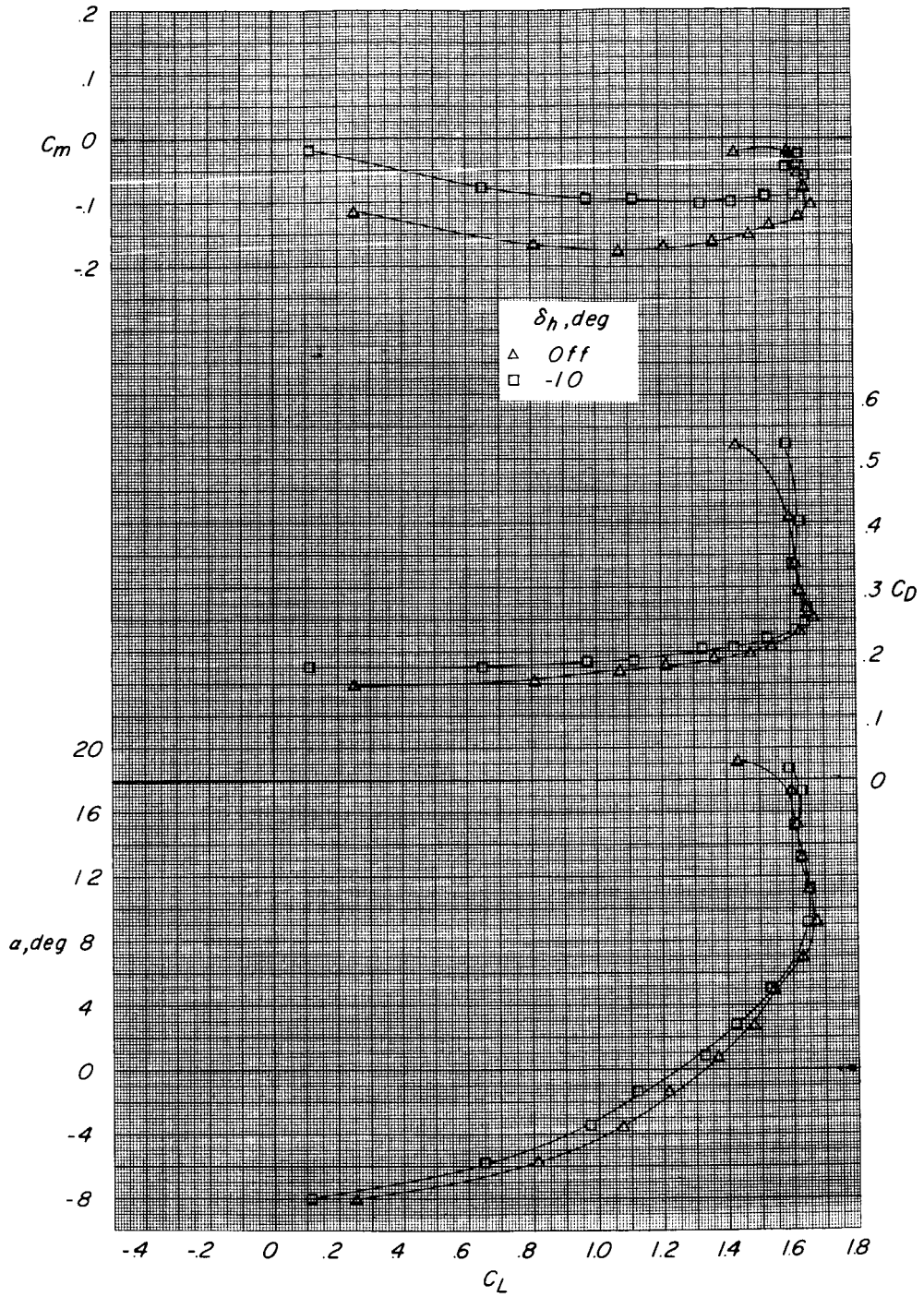
(b) $WF = 70^\circ s 0^\circ$.

Figure 12.- Continued.



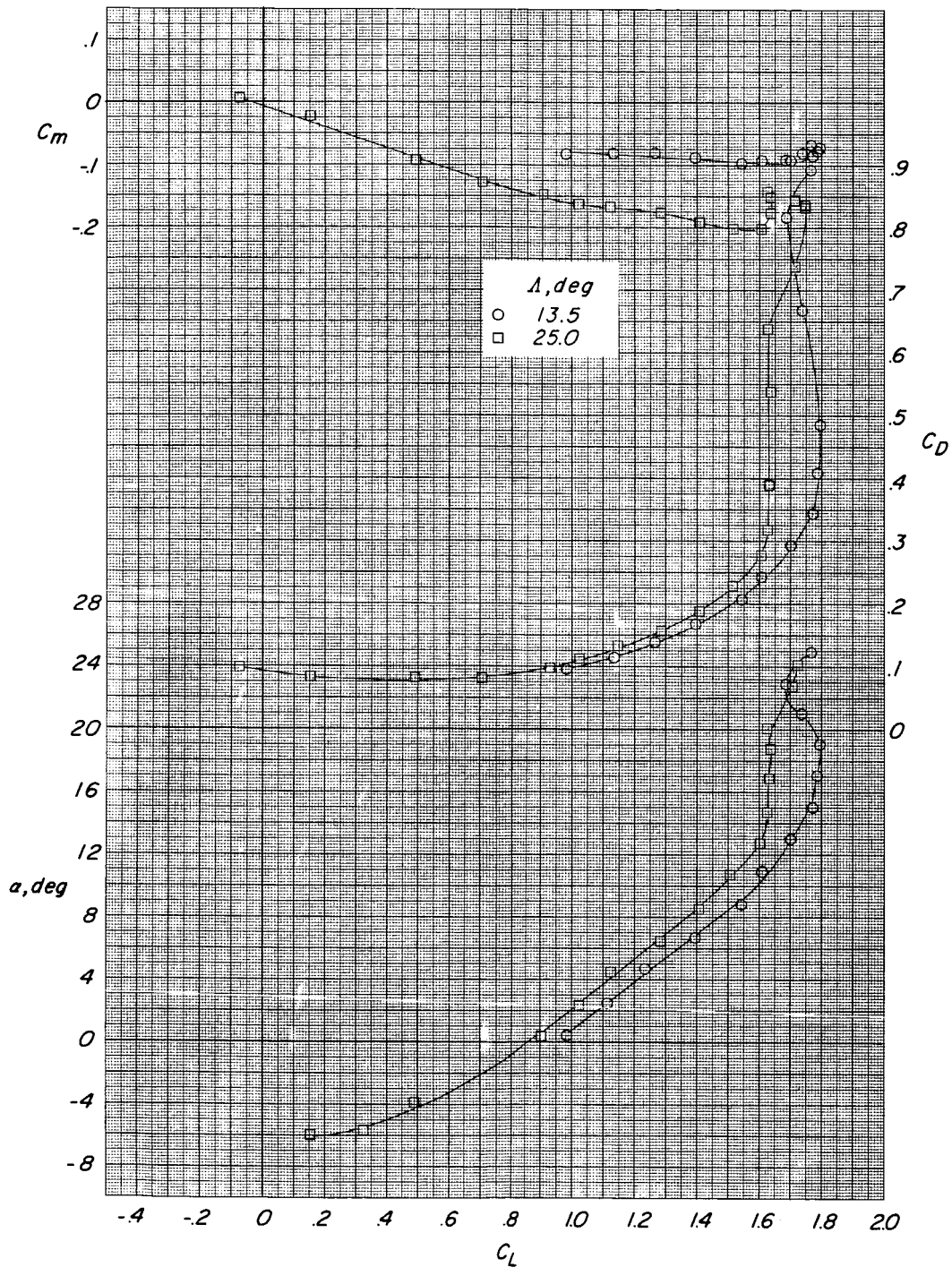
(c) $WF = 75^\circ s 0^\circ$.

Figure 12.- Continued.



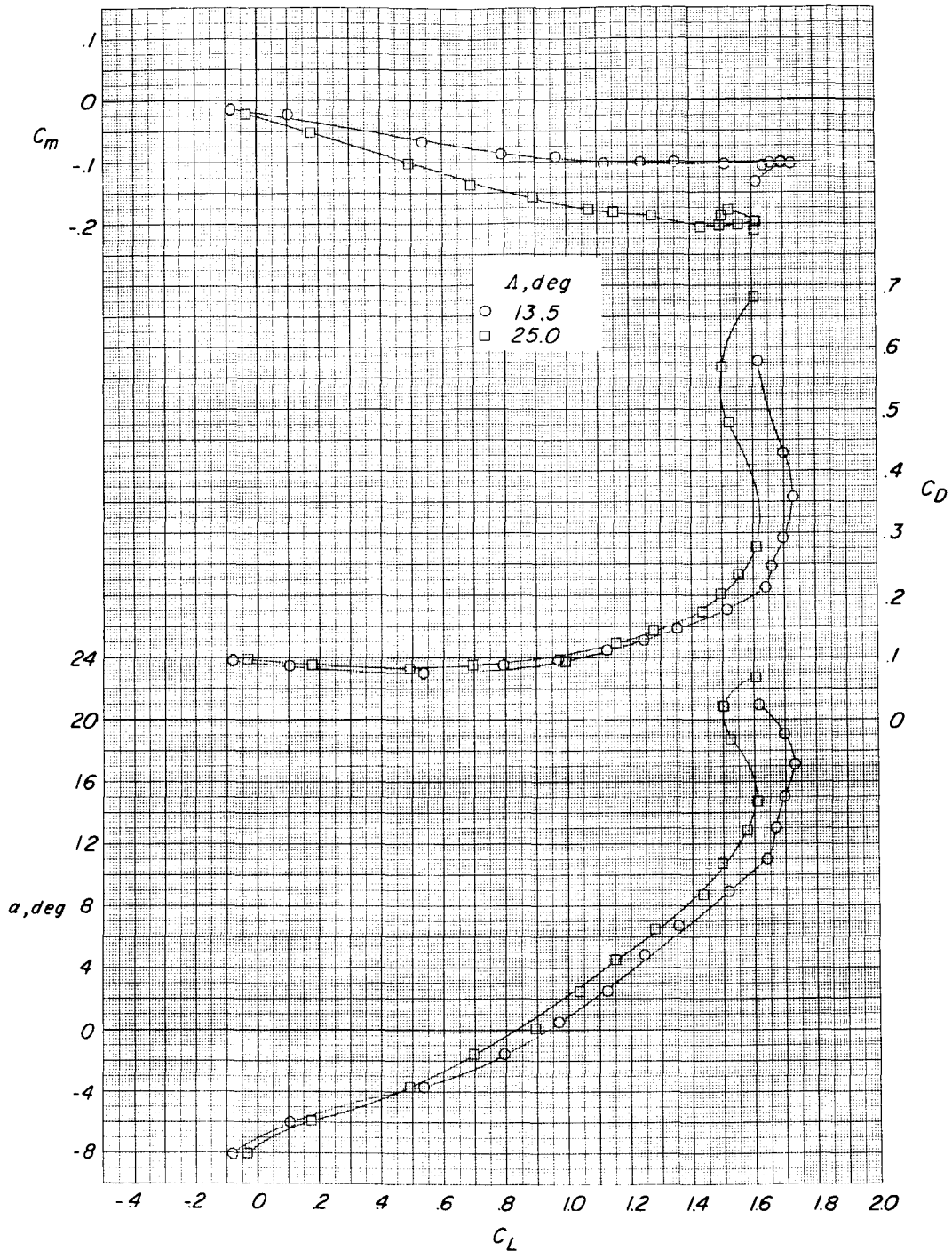
(d) $WF = 75^\circ s 45^\circ$.

Figure 12.- Concluded.



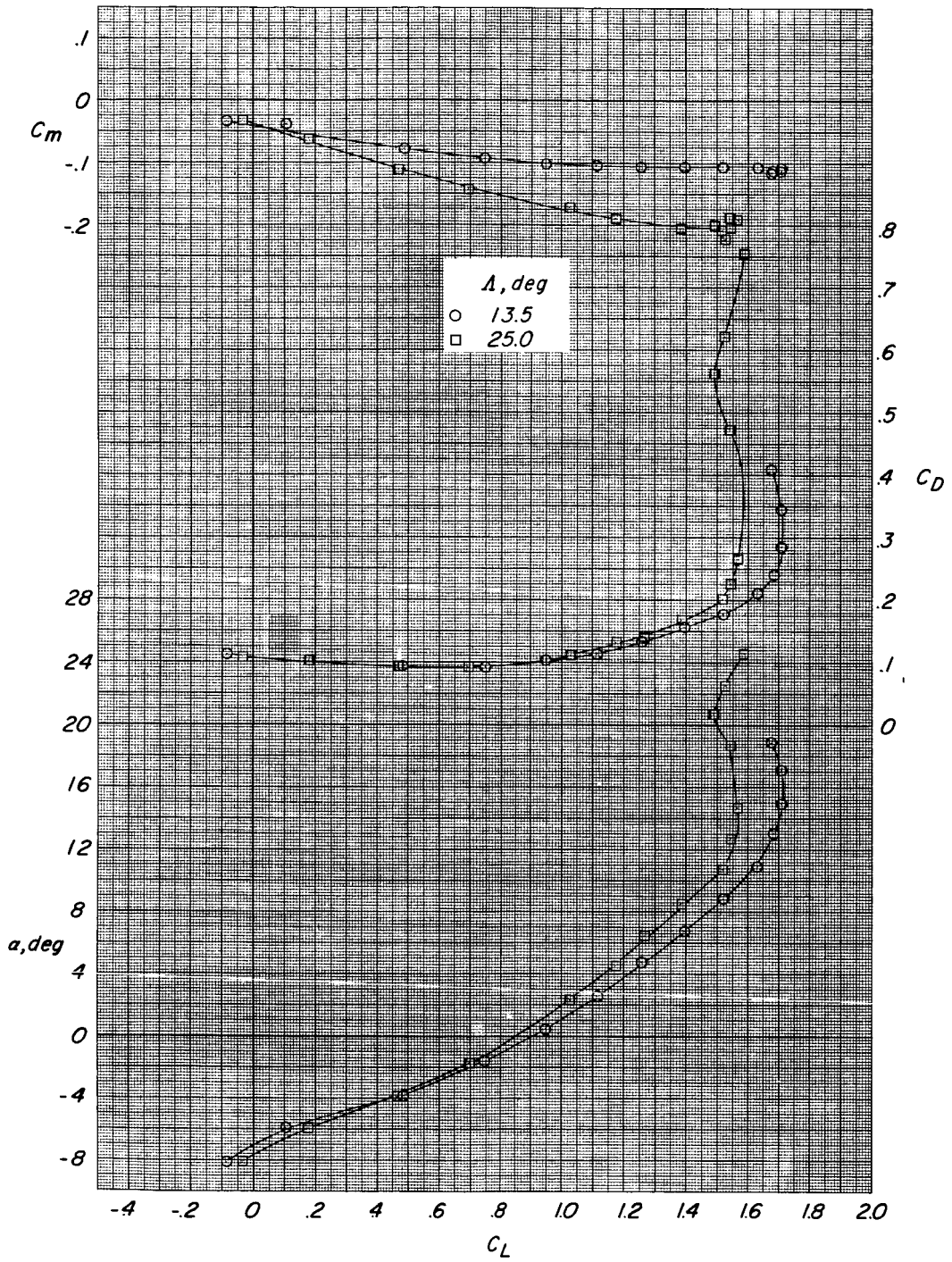
(a) $WF = 70^\circ s0^\circ$.

Figure 13.- Effect of wing sweep. $\delta_h = 0^\circ$; slat: $0.050c$; $0.020c$; $\delta_{dsf} = 30^\circ$.



(b) $WF = 70^\circ s 29^\circ$.

Figure 13.- Continued.



(c) $WF = 70^\circ S 45^\circ$.

Figure 13.- Concluded.

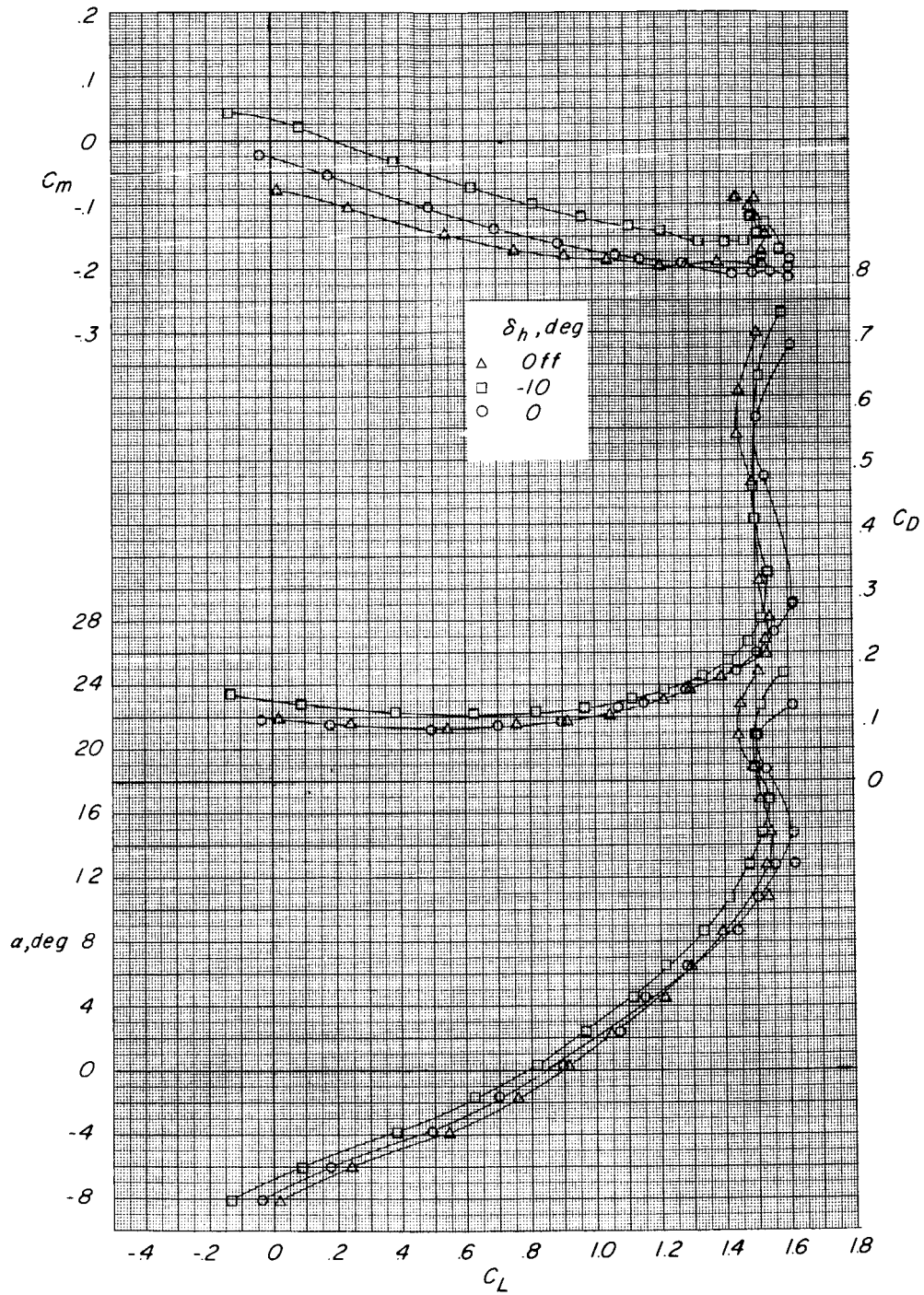


Figure 14.- Effect of horizontal tail. $\Lambda = 25^\circ$; $WF = 70^\circ s 29^\circ$;
 slat: $0.050c$; $0.020c$; $\delta_{dsf} = 30^\circ$.

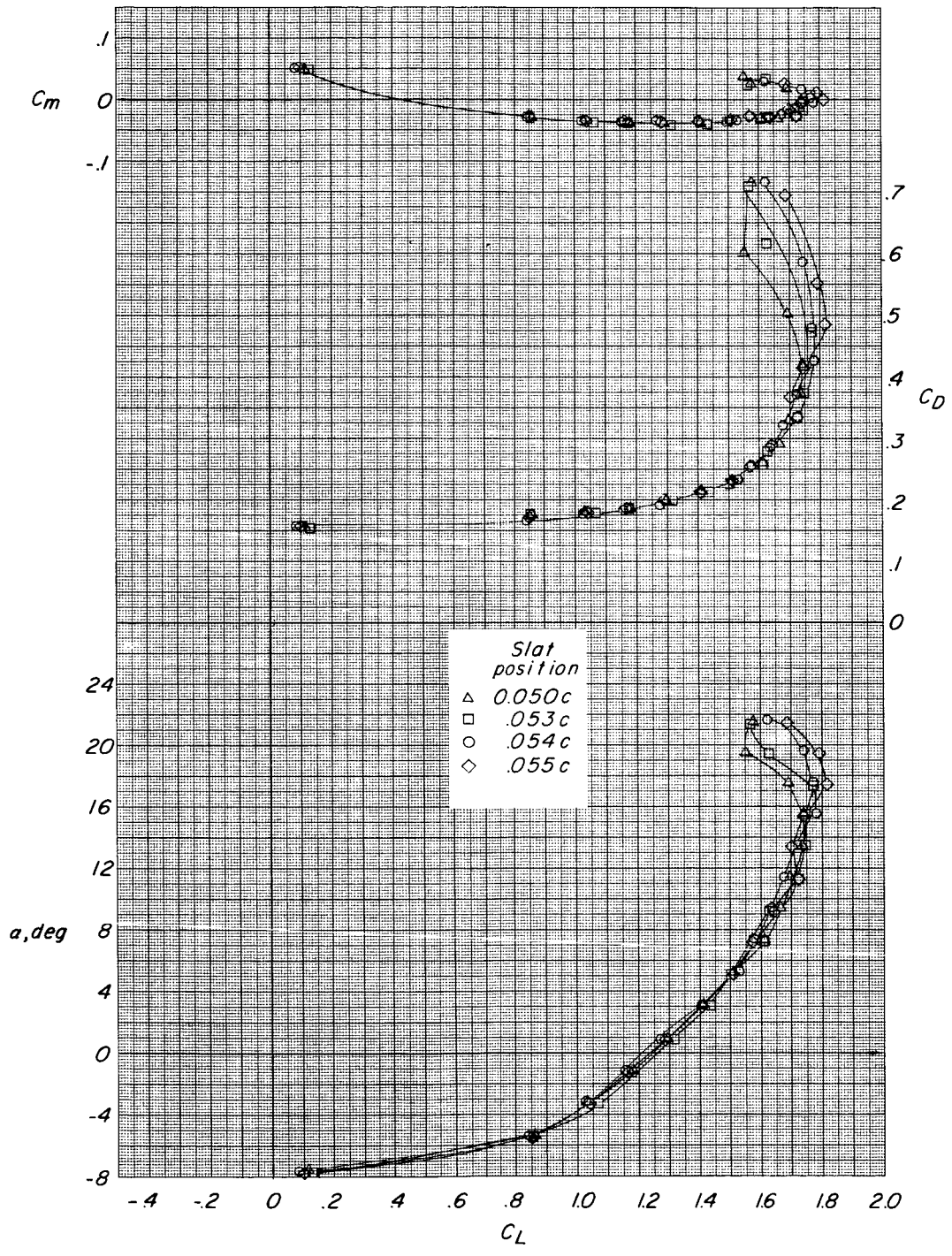


Figure 15.- Effect of slat leading-edge position. $\Lambda = 13.5^\circ$; $WF = 70^\circ s_0^\circ$; $\delta_h = 20^\circ$; slat gap = $0.018c$; $\delta_{dsf} = 50^\circ$.

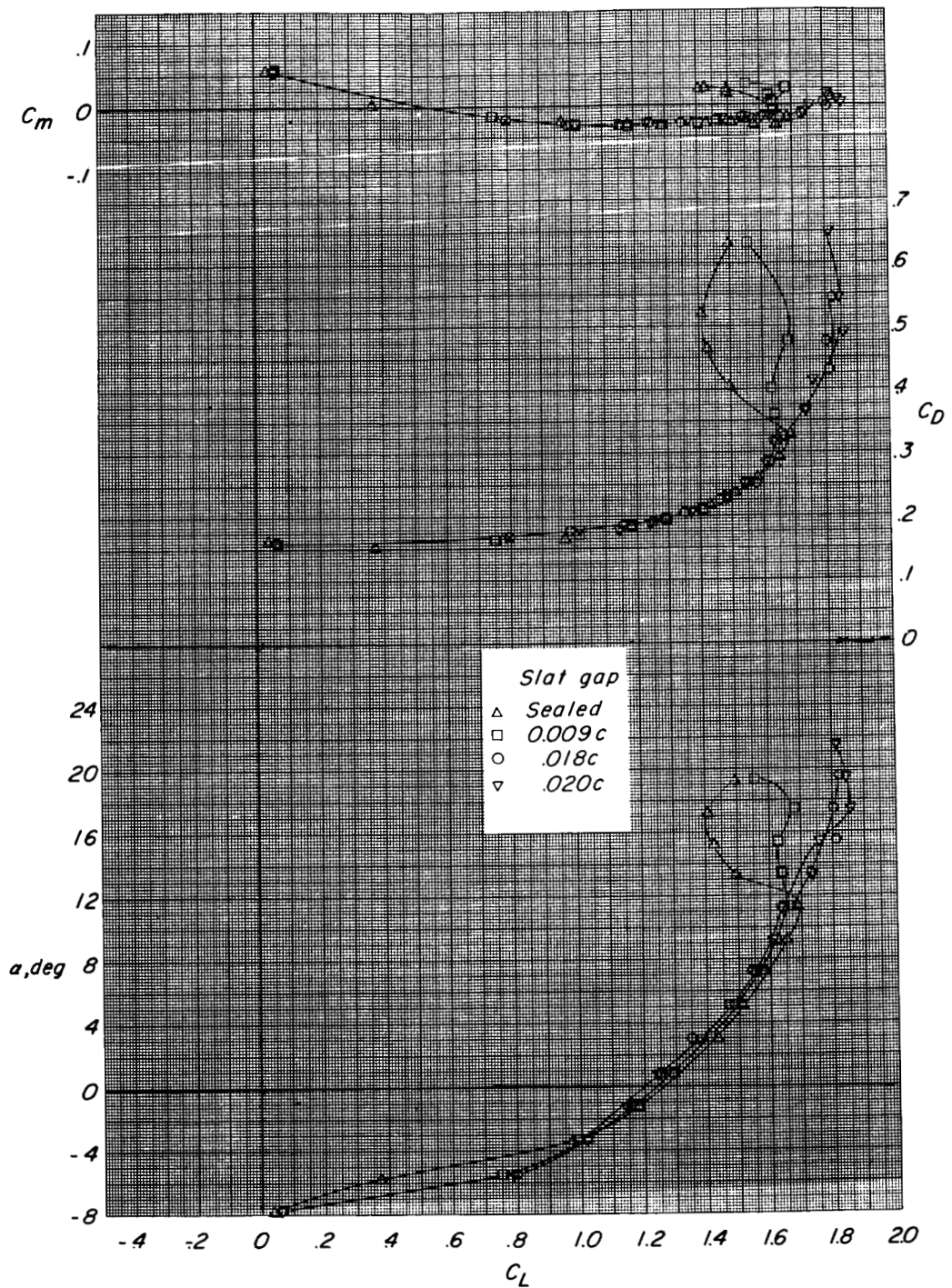


Figure 16.- Effect of slat trailing-edge gap. $\Lambda = 13.5^\circ$; $WF = 70^\circ$ so 0° ;
 $\delta_h = -20^\circ$; slat position = $0.050c$; $\delta_{dsf} = 50^\circ$.

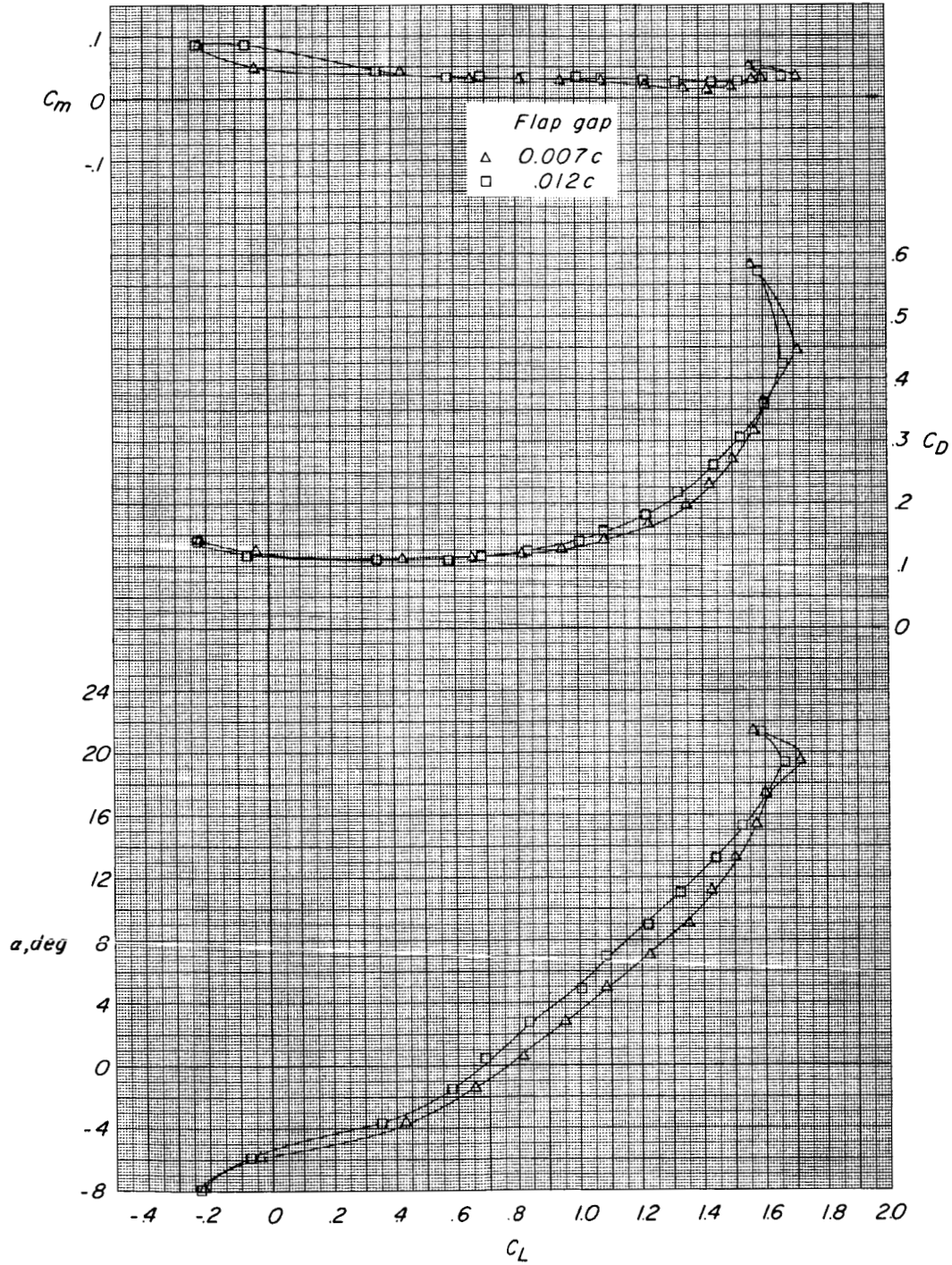


Figure 17.- Effect of trailing-edge flap gap. $\Lambda = 13.5^\circ$; $WF = 70^\circ s0^\circ$; $\delta_h = 10^\circ$; slat: $0.053c$; $0.018c$; $\delta_{ssf} = 40^\circ$.

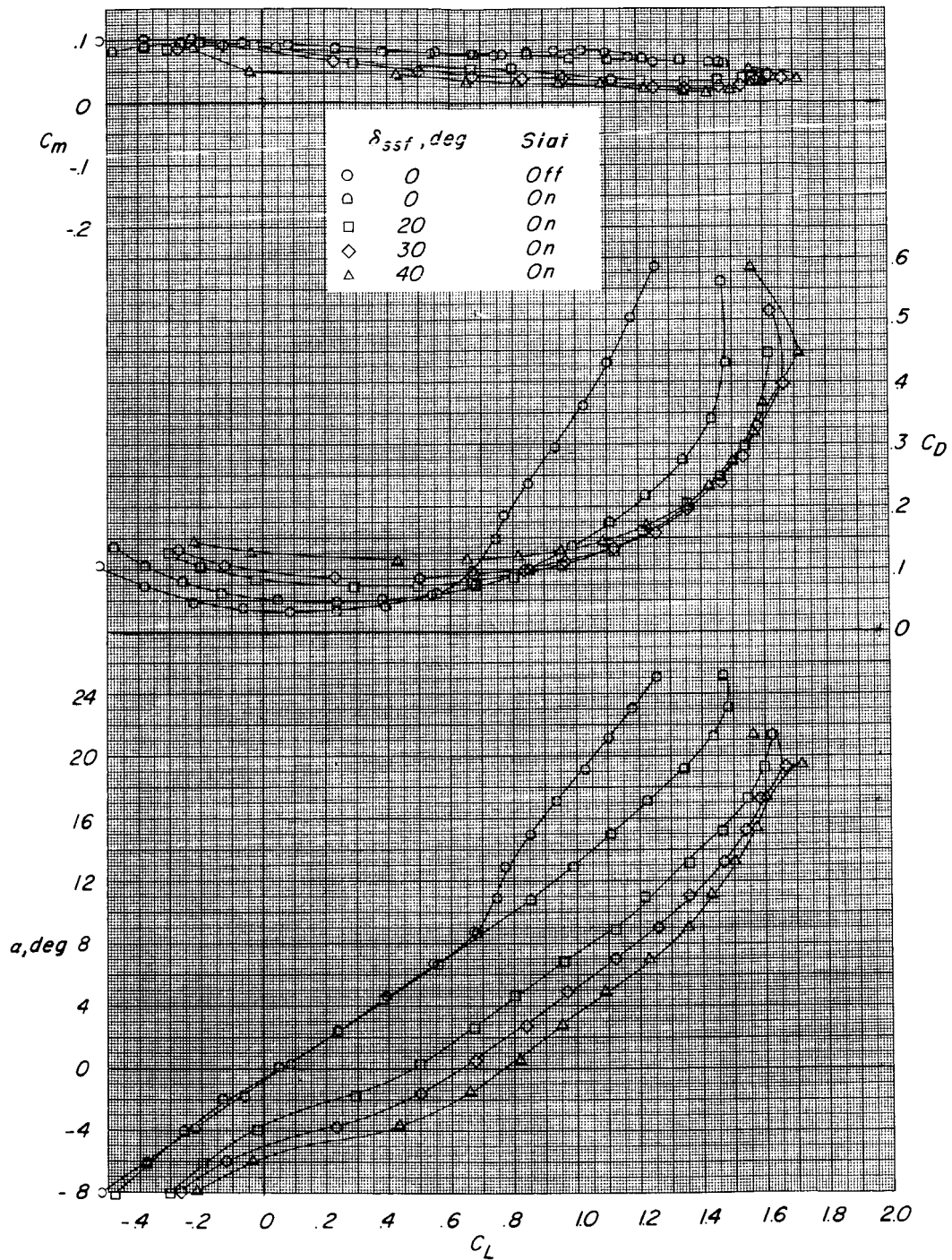


Figure 18.- Effect of leading-edge slats and single-slotted flap deflection.
 $\Lambda = 13.5^\circ$; $WF = 70^\circ s 0^\circ$; $\delta_h = -10^\circ$; slat: $0.053c$; $0.018c$; flap gap = $0.012c$.

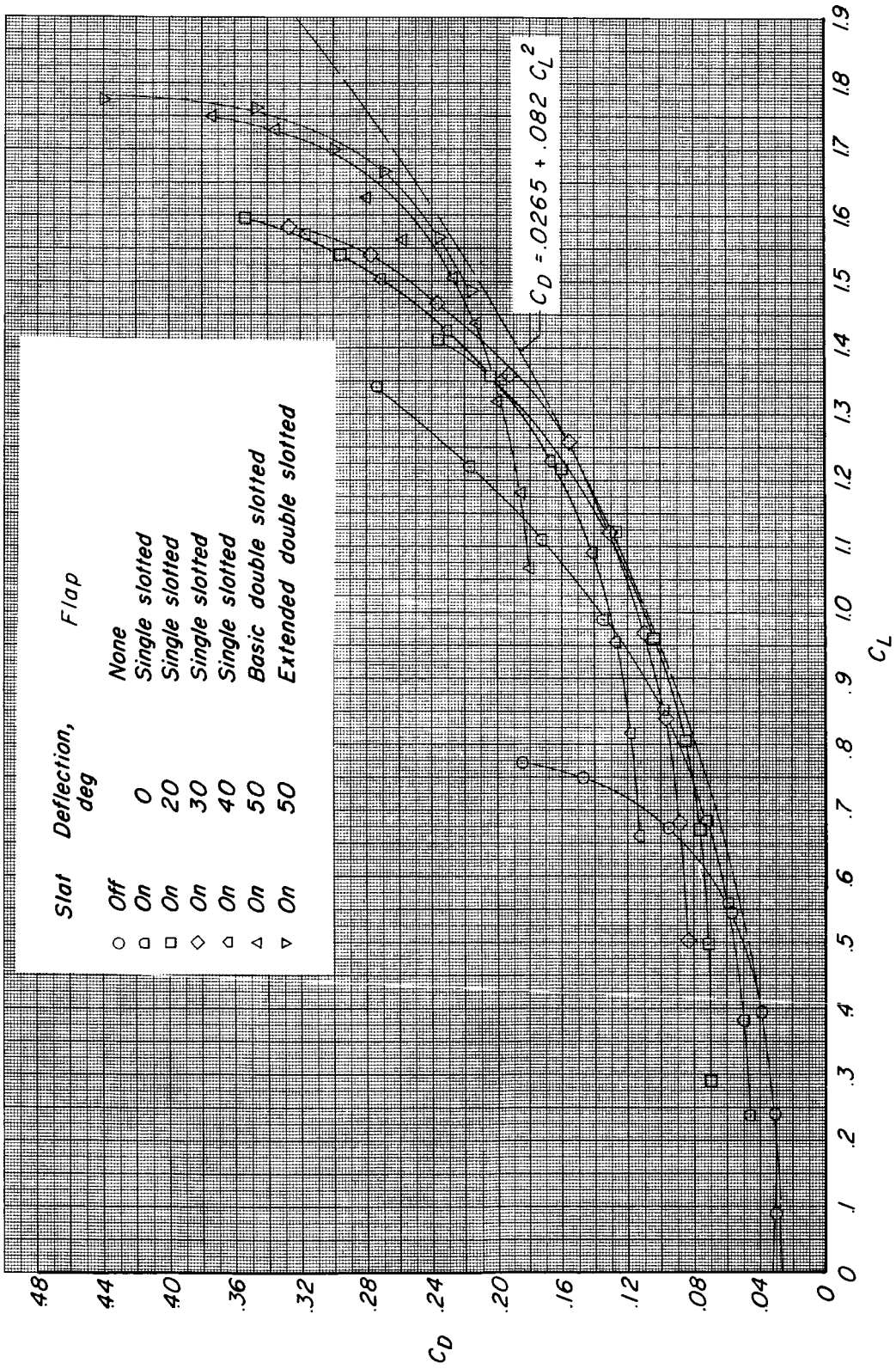


Figure 19.- Drag characteristics of several high-lift configurations.
 $\Lambda = 13.5^\circ$; $WF = 70^\circ$ to 80° ; $\delta_h = -10^\circ$; slat: $0.053c$; $0.018c$.

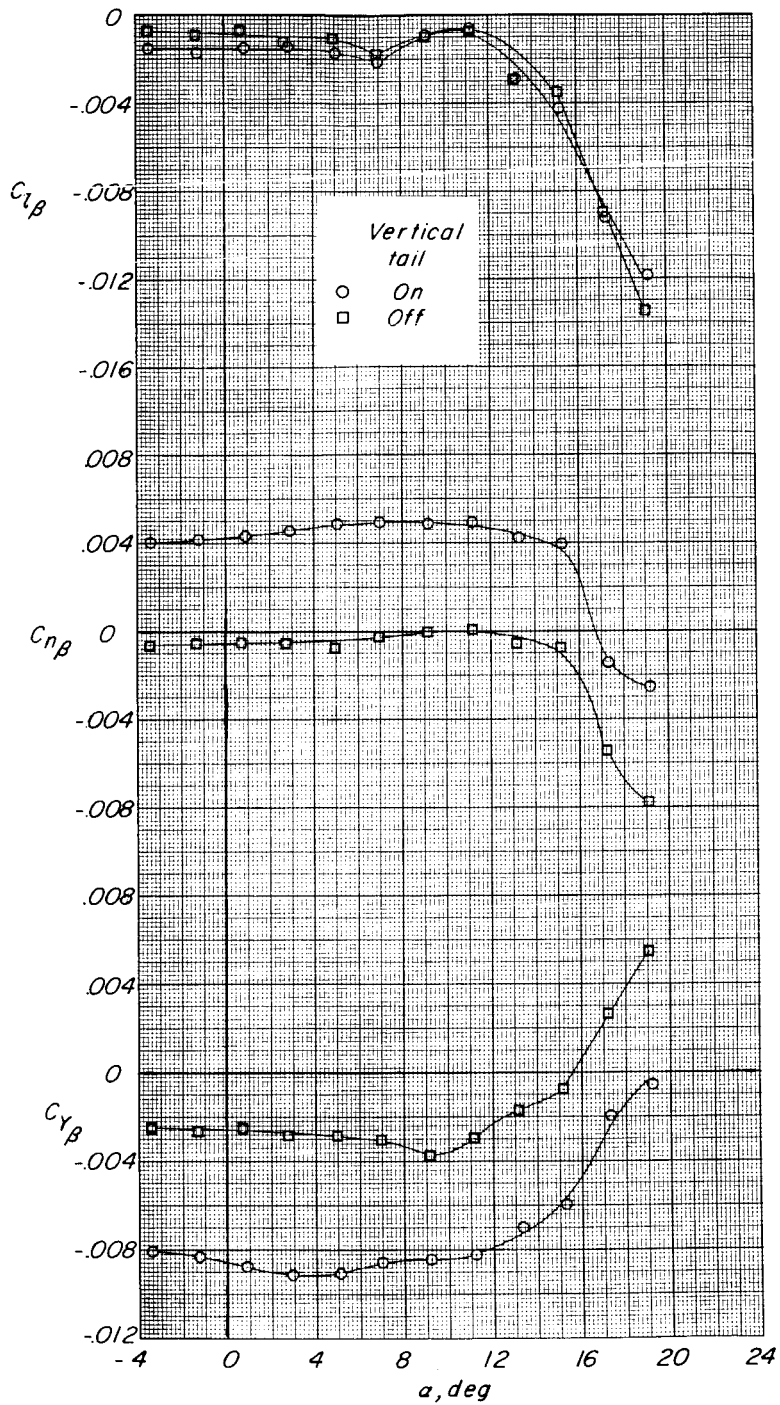


Figure 20.- Effect of vertical tail on lateral stability derivatives. $\Lambda = 13.5^\circ$; $WF = 70^\circ s 45^\circ$; $\delta_h = -10^\circ$; slat: 0.050c; 0.020c; $\delta_{dsf} = 50^\circ$.

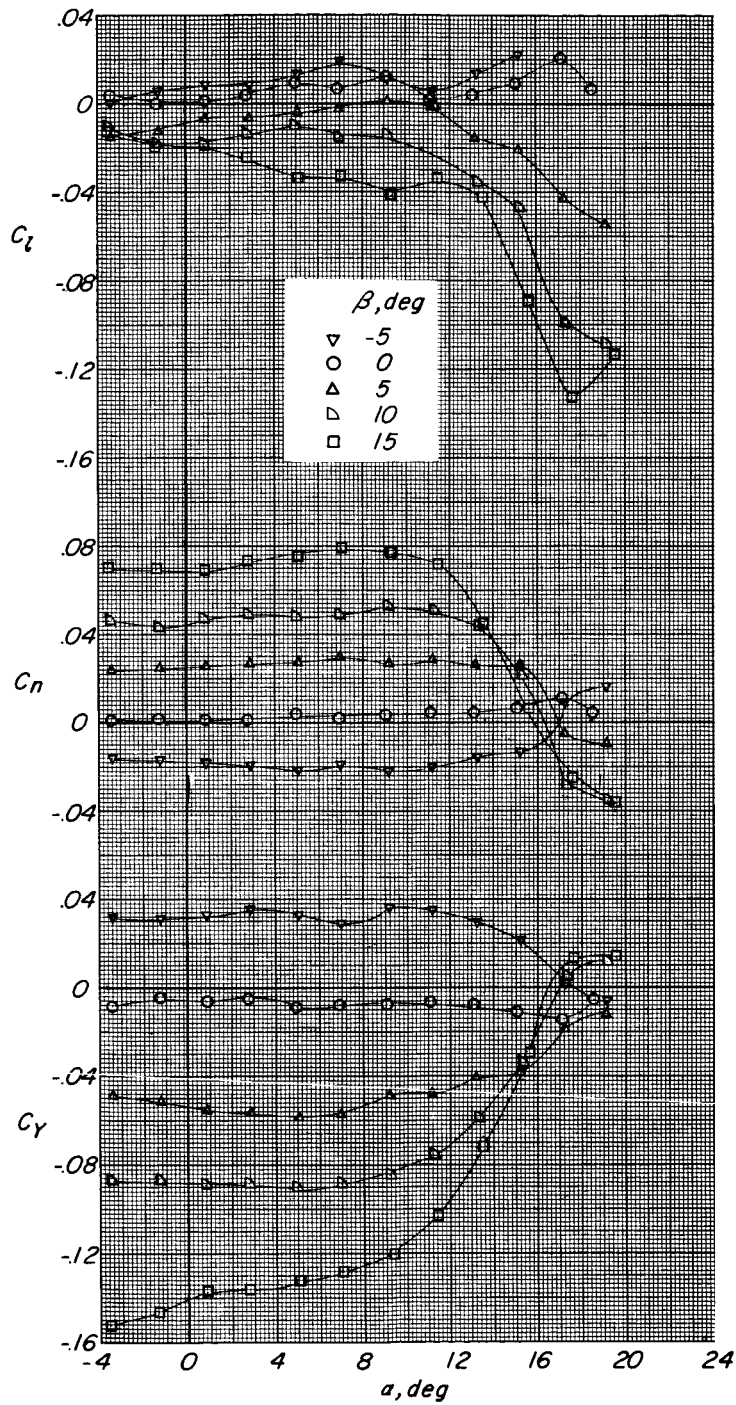


Figure 21.- Effect of sideslip angle on aerodynamic characteristics. $\Lambda = 13.5^\circ$;
 $WF = 70^\circ s 45^\circ$; $\delta_h = -10^\circ$; slat: $0.050c$; $0.020c$; $\delta_{dsf} = 50^\circ$.